NUMERICAL ANALYSIS OF INTEGRATED OPTICAL P-I-N PHASE MODULATOR

A Project Report

submitted by

M CHAITANYA KUMAR

in partial fulfilment of the requirements
for the award of the degree of

MASTER OF TECHNOLOGY

DEPARTMENT OF ELECTRICAL ENGINEERING
INDIAN INSTITUTE OF TECHNOLOGY MADRAS

May 2013

THESIS CERTIFICATE

This is to certify that the thesis titled **Numerical Analysis of Integrated Optical P-I-N Phase Modulator**, submitted by **M Chaitanya Kumar**, to the Indian Institute of Technology, Madras, for the award of the degree of **Master of Technology**, is a bonafide record of the research work done by him under my supervision. The contents of this thesis, in full or in parts, have not been submitted to any other Institute or University for the award of any degree or diploma.

Dr. Bijoy Krishna Das
Project Guide
Associate Professor
Dept. of Electrical Engineering
IIT-Madras, India, 600 036

Place: Chennai, India
Date: Tue 25th Jun, 2013

Dedicated to my parents

ACKNOWLEDGEMENTS

I would like to thank all those who supported me during my project work providing knowledge and suggestions. First of all, I would like to thank my project guide Dr.Bijoy Krishna Das, for giving this beautiful idea to work on and for his guidance. I would like to thank Sakthivel P , MS scholar and D. Dadavali for helping me obtaining Medici simulation results. I am also grateful to Varun Singh, Sujith Chandran and Shantanu Pal, Parimal Sah PhD scholars for their guidance and support. I express my gratitude to U Karthik, Saket Kaushal, Sidharth R, Harish Sasikumar, Meenatchi Sundaram, Rashmi Joshi and Sreevatsa Kurudi who are part of Integrated Optoelectronics Team at Department of Electrical Engineering. I would like to express my gratitude to PG senapathy computing resources at IIT Madras who have given me access to super computer Virgo for my project work.

ABSTRACT

The P-I-N waveguide phase modulator is an important component for on-chip optical modulation in SOI platform. This structure is basically single-mode rib waveguide region (intrinsic) with p-type and n-type impurities doped either side of it. Its electrical characteristics (carrier dynamics) are analyzed by semiconductor device simulator (mainly Poisson equation solver) and optical characteristics are evaluated by eigen mode solver (mainly Maxwell equation solver). The project objective is to understand the numerical techniques and to design a simulator with graphical user interface which can analyze the performance of P-I-N waveguide structures for any geometry of the rib waveguide.

The eigen mode solver developed at our lab has been adapted and modified to this program requirements and integrated with electrical simulator. Our simulator has shown L_π(Length required for π phase in optical signal) of around 250 μm for the dimensions of rib height of 4.5 μm, slab height of 3 μm,rib width of 4 μm. It shows the figure of merit less than 0.27 V-mm which is considerable and close to the practical results.

TABLE OF CONTENTS

LIST OF TABLES

LIST OF FIGURES

ABBREVIATIONS

Acronyms

BMFET	Bipolar Mode Field Effect Transistor
CMOS	Complimentary metal-oxide semiconductor
FDM	Finite Difference Method
GUI	Graphical User Interface
MOS	Metal-oxide semiconductor
SRH	Shockley Read Hall
TE	Transverse Electric (polarization)
TM	Transverse Magnetic (polarization)
Si	Silicon
SiO_2	Silicon dioxide

Units

MHz	Mega Hertz
μm	Micrometer
ns	Nano Second
A	Ampere
V	Volt
mm	milli meter

NOTATION

n	Refractive index
n_{eff}	Effective refractive index
ϵ	Permittivity
L_{pi}	Length for achieving π phase
α	Absorption coefficient
n, p	Electron and Hole concentrations
(i, j)	represents the node at (i,j) incremental distance from origin
V	Potential
δ	correction factor
l	unique ID assigned to all nodes in 2 Dimensional structure
t_{dr}	Dielectric relaxation time

CHAPTER 1

Introduction

1.1 Background

The science of Photonics involves generation, transmission, detection of photons as which acts as the information carriers. The main advantages of optical communication are high bandwidth, low loss. **Silicon Photonics** is the technology involved with producing photonic devices, which are fabricated by CMOS compatible process flow. With the technological developments in electronics industry, the device dimensions are reducing. After a threshold limit, the electrical interconnect delay has become the primary bottleneck for achieving high bandwidth. One of the solution to overcome this problem is to go for optical interconnects which is possible with silicon photonics.
One of the essential components in silicon photonics are optical modulators, which are necessary to convert the electrical signals into optical signals. "Plasma Dispersion effect" is most common technique used to achieve the phase modulation which is obtained through change in refractive index via variation in mobile carrier concentration i.e., electrons and holes. The Drude model is used to derive an analytical expression for absorption, α. This change in absorption leads to a change in the complex refractive index. The equation(Drude-Lorentz equation [1]), relating the change in electron and hole concentration to the absorption is,

$$\Delta\alpha = \frac{e^3\lambda_0^2}{4\pi^2c^3\epsilon_0 n}\left(\frac{N_e}{\mu_e(m_{ce}^*)^2} + \frac{N_h}{\mu_h(m_{ch}^*)^2}\right) \tag{1.1}$$

and the corresponding equation for change in real part of refractive index(Δn) is,

$$\Delta n = \frac{e^2\lambda_0^2}{8\pi^2c^2\epsilon_0 n}\left(\frac{N_e}{m_{ce}^*} + \frac{N_h}{m_{ch}^*}\right) \tag{1.2}$$

N_e, N_h are the electron and hole concentrations, μ_e, μ_h are the electron and hole mobilities, m_{ce}^*, m_{ch}^* are the electron and hole effective masses respectively. e is the electron

charge. λ_0 is the free space wavelength 1.55 μm. ϵ_0 is the free space permittivity and n is the refractive index.

An empirical fit for Δn, $\Delta \alpha$ was produced by Soref and Benette, which was found to be in close agreement with that predicted by the Drude-Lorentz equation (1.1) and (1.2). At λ = 1.55 μm, which is the wavelength of interest for us,the relations are,

$$\Delta n = \Delta n_e + \Delta n_h = -[8.8 \times 10^{-22} \Delta N_e + 8.5 \times 10^{-18} (\Delta N_h)^{0.8}] \tag{1.3}$$

$$\Delta \alpha = \Delta \alpha_e + \Delta \alpha_h = [8.5 \times 10^{-18} \Delta N_e + 6.0 \times 10^{-18} \Delta N_h] \tag{1.4}$$

where $\Delta N_e, \Delta N_h$ are the change in electron and hole concentrations respectively.

The mach-zehnder interferometer(MZI) is shown in Figure 1.1. The continuous signal is split into two arms of MZI. One of the arms were doped with p type (mainly boron) and n type (mainly phosphorous) impurities. We make sure to get the phase shift of π by applying sufficient voltage. The phase modulation will be converted into intensity modulation by destructive interference at the junction and hence, we get intensity modulated wave.

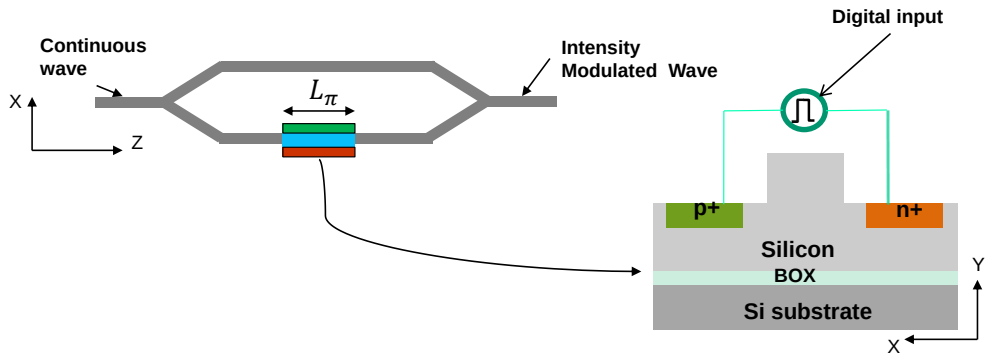

Figure 1.1: Mach-zender Interferometer with p-type and n-type impurities

To obtain free carrier concentration variation in silicon, four major techniques have been implemented by several authors and are listed below.

1) Carrier injection in PN/PIN diode (forward bias) [2]

2) Carrier plasma shift in BMFET(Bipolar mode field effect transistor) [3]

3) Carrier accumulation in MOS Capacitor [4]

4) Carrier depletion in PN/PIN diode (reverse bias) [5]

In this report, we mainly emphasis on solving for electrical and optical characteristics of Carrier injection modulators.

1.2 Project Motivation

In order to understand the characteristics of Silicon photonic devices, we need to solve the device structure using Laplace (electrostatic characteristics for insulator), Poisson (electrostatic characteristics for semiconductor region), Eigen mode (for optical characteristics of entire structure), transport and continuity (carrier movement information for semiconductor region) equations.
Before fabricating the device, it is important to design the waveguide geometry, electrode positions, doping distributions to obtain the optimized performance.
The conventional approach is to use a simulation tool (RSoft-BeamProp) to get the optimized dimensions for optical field confinement. Considering these dimensions, we simulate the waveguide in semiconductor device simulation tool to get electrical characteristics. With the help of Soref experimental fit as explained with equations 1.3 and 1.4, we find the corresponding refractive index variation for the geometry. Considering this refractive index as input to another simulator tool RSoft-Femsim, we obtain the field confinement and effective index under equilibrium and for applied bias.
This complete process need to be repeated if we need to change the dimensions or electrode width. In most cases, we can not get the Poisson solver and Eigen mode solver in single package. Moreover, it is important to know the numerical techniques for solving the equations. This served as the motivation to develop a numerical simulator for computing both electrical and optical characteristics of P-I-N based silicon optical modulators.

1.3 Research objective

The objective is to develop a numerical simulator which shows the electrical and optical characteristics of a particular waveguide simultaneously and to show the variation of

design parameters with respect to electrode offset and width, doping distribution on a Graphical user interface(GUI). The platform used was Matlab with uniform finite difference technique .

The P-I-N based carrier injection modulators have already been demonstrated in our lab. Based on suggestions considered, we have implemented the numerical simulator. The simulated results were in accordance with the experimental results.

1.4 Thesis Organization

The thesis work contains four chapters. Second chapter consists of device simulation algorithm at equilibrium and applied bias which were explained in detail. Followed by, simulation and results including the graphical user interface. In final chapter, we discussed about summary and future work.

CHAPTER 2

P-I-N waveguide structures : Numerical building blocks

As explained earlier chapter, The optical modulation can be achieved by considering single mode waveguide structure [6] with sufficient doping concentration enough to change the effective index of the optical mode. Figure 1.1 shows the rib waveguide structure which is used for guiding the optical signal. The structure we considered for simulation is shown in Figure 2.1. Doping distribution is considered to be gaussian function. Junction depth is considered to be 1 μm for both P and N regions. In this chapter, we explain the algorithm design to solve the structure, Poisson equation solution at equilibrium, eigen mode equation at equilibrium, poisson equation solution in quasi equilibrium with help of transport-continuity equations ,solution of eigen mode equation at applied bias, followed by transient electrical characteristics.

We have chosen the device dimensions satisfying the single mode condition.

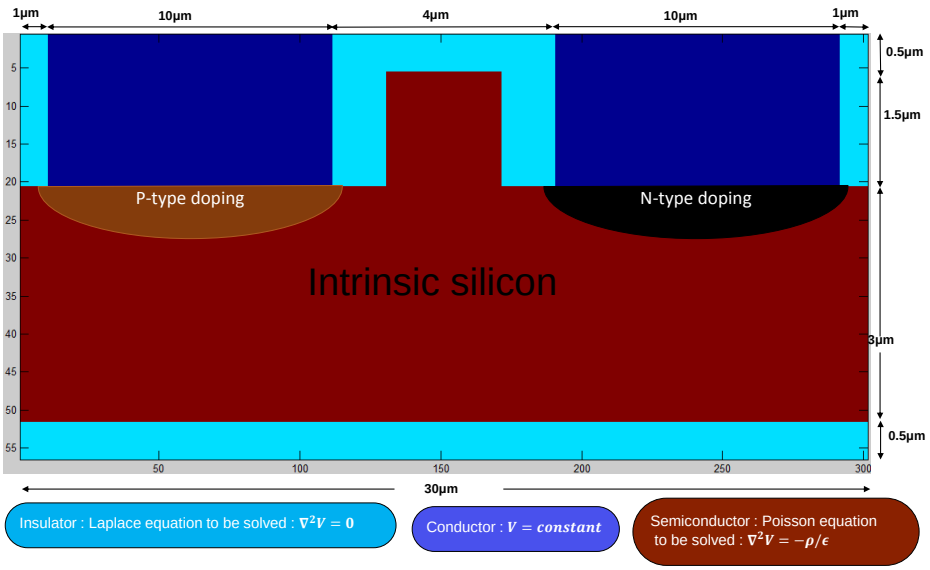

Figure 2.1: SOI rib waveguide structure

2.1 Algorithm for simulation

The procedure is explained through flow chart. Left column explains the inputs necessary for each step to execute. Right column indicates the output we get from that step. The mesh size of the structure is taken as minimum of Debye length and $\frac{1}{10}\lambda$.

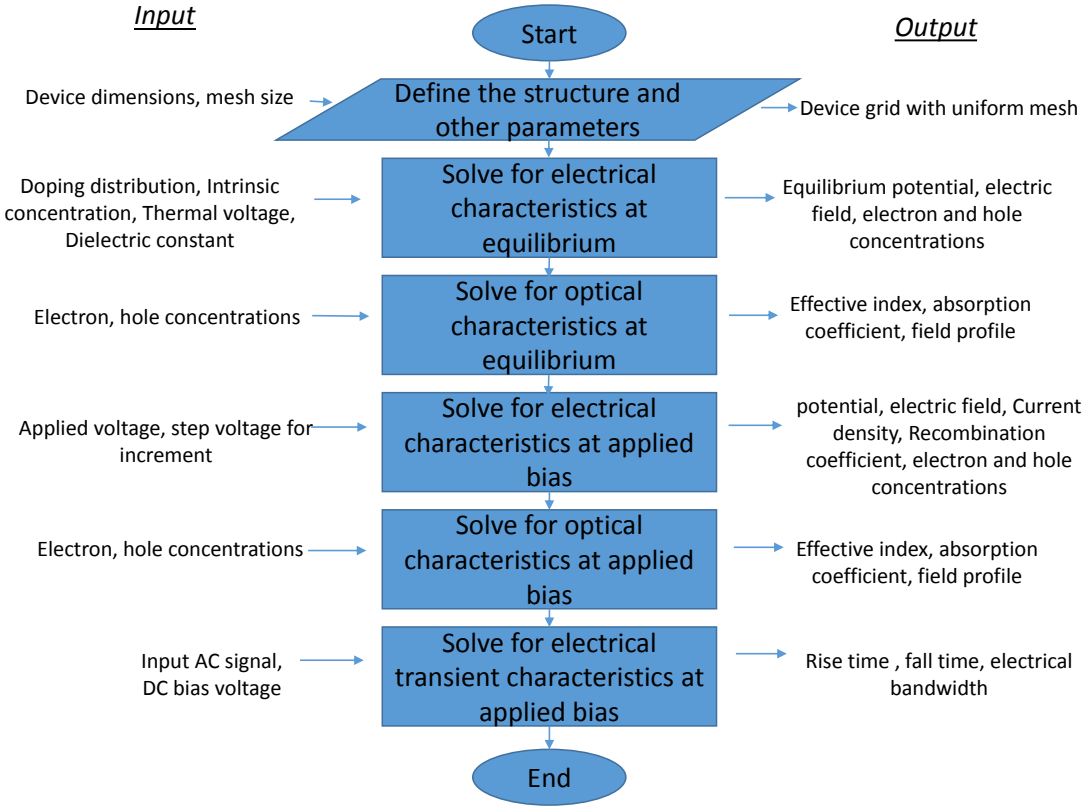

Figure 2.2: Flowchart for extracting the electro-optic effects of waveguide

Debye length is defined as, $L_D = \sqrt{\frac{\epsilon \times V_t}{q \times N}}$ [13]
where ϵ is permittivity of the medium. V_t is the thermal voltage $0.026eV$ at room temperature. q is the electron charge. N is the impurity concentration.

2.2 Assumptions considered

Before proceeding to the detailed explanation of the algorithm for solving the structure, we need to address some of the assumptions considered for solving the structure since the equations are specific to homogeneous semiconductor material Si.

Boltzmann approximation:

When the individual Si atoms brought nearer to form crystalline silicon, the discreet energy levels in the atoms form a continuous band. When the equilibrium is attained, this band splits to form conduction band(upper band which has empty energy states) and valance band(lower band and filled energy states) and they will be separated by energy gap [11].

At T = 300K , the resulting thermal energy will be sufficient to break the Si-Si bonds to produce electron-hole pair. This phenomenon is called **Thermal Generation**. To increase the conductivity, we will dope the intrinsic silicon with impurities of p or n type which makes it extrinsic semiconductor. At T = 300K, we will have majority and minority carriers because of the extra carriers obtained from ionization of impurities. This phenomenon can be described as **Impurity ionization**.
When we form P-N junction, the Fermi levels align so as to reach equilibrium. The energy band diagram is shown in Figure 2.3.

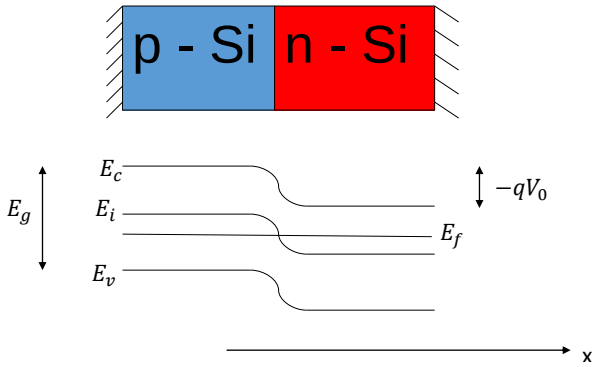

Figure 2.3: Energy band diagram of P-N junction semiconductor. E_c is the conduction band minimum energy level. E_ν is the valance band maximum energy level. E_i is the intrinsic energy level. E_g indicates the energy gap. E_f is the fermi level at equilibrium. V_0 is the built-in potential. The energy levels are always meant to be electron energy. The potential is considered to be for positive charge. Hence we represent the E-V relationship with negative sign.

The electron and hole concentrations can be written as [11]

$$\begin{aligned} n &= n_i e^{\frac{E_{fn}-E_i}{kT}} \\ p &= n_i e^{\frac{E_i-E_{fp}}{kT}} \end{aligned} \tag{2.1}$$

where n, p represent electron and hole concentrations respectively. n_i is intrinsic concentration. E_{fn}, E_{fp} are the quasi-fermi levels of n-type and p-type semiconductors. At equilibrium, both are equal to E_f. kT is thermal energy at room temperature and typically $0.026eV$. E_i is the intrinsic level and is at the mid level of the conduction and valance bands.

Constant temperature:

The temperature is assumed to be constant at 300K i.e., there is no effect of temperature gradient.

Neglecting surface state effects:

Surfaces have different behavior compared to the bulk region. We assume these effects are absent. However, we consider that there are infinite number of recombinations at conductor-semiconductor junction.

Complete ionization assumption:

We assume that the impurities are completely ionized at room temperature T= 300K.

Concentration dependent mobility:

Mobility of the carrier is dependent on ionized impurity concentration, electric field, carrier-carrier interactions. For this simulation purpose, we consider only the concentration dependent mobility.

Presence of Shockley-Read-Hall recombination

The recombination rate is always equals generation rate at equilibrium. The recombination are mainly of three types.
1.Direct band-band recombination
2.Indirect recombination

3.Auger recombination

Since Silicon is an indirect band gap semiconductor, the recombination occurs through **trapping**. we consider Shockley-Read-Hall or SRH theory to explain and implement the continuity equation. The direct band-band recombination is negligible in Silicon material. At high doping, we need to include the Auger recombination effects which were not included here. Taking SRH theory into consideration, Generation-Recombination coefficient is defined as,

$$U = \frac{np - n_i^2}{\tau_p(n + n_1) + \tau_n(p + p_1)} = -g \tag{2.2}$$

where U is net recombination rate , g is net generation rate, n is electron concentration, p is hole concentration, $n_1 = n_i e^{\frac{E_t - E_i}{kT}}; p_1 = n_i e^{\frac{E_i - E_t}{kT}}$ where E_t is the trap energy level. τ_p, τ_n are the hole and electron life times . The below is the modeled equation considered for the simulation [13].

$$U = \frac{(np - n_i^2)}{(n + p + (2n_i))} \frac{1}{[(5 \times 10^{-5})/(1 + ((N_A + N_D)/(5 \times 10^4)))]} \tag{2.3}$$

Relaxing the electrode effects on optical mode

When we solve for optical characteristics, the conductor electrode affects the optical field profile. In this case, we consider that the metal electrodes are at sufficient distance from the rib structure and hence they are not considered here while solving for optical characteristics.

2.3 Electrical characteristics at equilibrium -Poisson/Laplace equation

The **Gauss law** states that the total electric flux through any closed surface is equal to the total charge enclosed by that surface [7].

If we assume that the medium is linear (the electric flux density D is linear to the electric field E), homogeneous (ϵ is constant within the structure) and isotropic (D and E have

same direction), the Poisson equation can be written as,

$$\nabla^2 V = -\rho/\epsilon \tag{2.4}$$

If the close surface does not have any charge density , the poisson equation will become Laplace equation. In 1D, equation 2.4 can be represented as,

$$\frac{d^2V}{dx^2} = -\rho(x)/\epsilon \tag{2.5}$$

One of the techniques to solve the above equation is by **finite difference scheme** by central difference method.These finite difference approximations are algebraic in form. They relate the value of the dependent variable at a point in the solution region to the values at some neighboring points [8]. The solution is obtained through these basic steps.

1. Descretize the region by choosing proper mesh size as explained in 2.1.
2. Approximate the equation into discretized form relating the dependent variable at a point to its values at neighboring points.
3. Apply initial condition and boundary conditions to the discretized equation.
4. Update the dependent variable at all points in the region and solve the equation again till the norm of the difference of last two iterative solutions reach a tolerance value which in this case is, 10^{-5}.

In 2D the equation 2.4 can be written as,

$$\frac{d^2V}{dx^2} + \frac{d^2V}{dy^2} = \frac{-\rho}{\epsilon} \tag{2.6}$$

The ρ in this equation is the net charge density which is dependent on dependent variable, in this case the electric potential. Hence, it is called as non-linear poisson equation. The algorithm that is followed is known as Gummel method [13].
With the discretization scheme mentioned, we can rewrite the above equation as,

$$V(i+1,j)+V(i-1,j)+V(i,j-1)+V(i,j+1)-4V(i,j) = \frac{-\rho(i,j)\times h^2}{\epsilon} \tag{2.7}$$

where h is the mesh size of the structure, ϵ is the permittivity of the structure, i implies that node at a distance of $i \times h$ horizontal distance from origin, j implies node at a

distance of $j \times h$ vertical distance from origin or the reference point.

This equation implies that the potential at a node in the region is different from the averaging potential from the neighboring nodes by a factor which is proportional to the charge density at that node. For this case, the neighbors either horizontal or vertical with respect to the current node by one incremental distance h are considered for solution.

The discretized poisson equation is,

$$\begin{aligned} V(i+1,j) + V(i-1,j) + V(i,j-1) + V(i,j+1) - 4V(i,j) &= \frac{-\rho(i,j) \times h^2}{\epsilon} \\ &= \frac{-(p(i,j) - n(i,j) + N_D(i,j) - N_A(i,j)) \times h^2}{\epsilon} \end{aligned} \tag{2.8}$$

And the discretized Laplace equation is,

$$V(i+1,j) + V(i-1,j) + V(i,j-1) + V(i,j+1) - 4V(i,j) = 0 \tag{2.9}$$

represents that the potential at the current node can be found by averaging the potentials at neighboring nodes.

We need to solve the laplace equation for insulator region, Poisson equation for semiconductor and constant potential for conductor region simultaneously in order to obtain the simulation characteristics.

The procedure to solve these equations is explained below.

2.3.1. Initialization:

In this step, we initialize the potential of the **semiconductor region** using the charge neutrality condition [9] and potential at the insulator nodes are initialized to zeros.

$$n(i,j) - p(i,j) = N_D(i,j) - N_A(i,j) \tag{2.10}$$

By boltzmann approximation explained in 2.2,taking E_f as reference energy level and $E_i = -qV$ and simplifying, the equation can be written as,

$$V(i,j) = 2 \times V_t \times sinh^{-1}\Big(\frac{N_D(i,j) - N_A(i,j)}{2n_i}\Big) \tag{2.11}$$

The above obtained matrix is considered as initial guess for potential.Similarly mobility for electrons and holes were also initialized based on impurity concentrations N_D, N_A.

2.3.2. Applying Dirichlet condition at metal interface:

Since conductor is an equipotential surface, we need to initialize the potential value at the conducting surface to the potential at semiconductor surface.

2.3.3. Calculating the coefficients of Poisson/Laplace equation:

The potential for solving poisson equation is taken as $V + \delta$ and substituted into 2.8 along with botlzmann equation 2.2 [13] and the complete equation can be written as,

$$\begin{aligned}\delta(i+1,j)+\delta(i-1,j)+\delta(i,j-1)+\delta(i,j+1)+\delta(i,j)(-4-\frac{qh^2n_i}{\epsilon V_t}(e^{-V(i,j)}+e^{V(i,j)}))\\ +V(i+1,j)+V(i-1,j)+V(i,j-1)+V(i,j+1)-4V(i,j)\\ =\frac{-qh^2}{\epsilon V_t}(n_ie^{-V(i,j)}-n_ie^{V(i,j)}+N_D(i,j)-N_A(i,j))\end{aligned} \tag{2.12}$$

This equation along with Laplace equation can be generalized as,

$$\begin{aligned}a(i,j)\delta(i-1,j)+b(i,j)\delta(i,j)+c(i,j)\delta(i+1,j)\\ +d(i,j)\delta(i,j-1)+e(i,j)\delta(i,j+1)=k(i,j)\end{aligned} \tag{2.13}$$

The matrices a, b, c, d, e are 2 dimensional and are either constants or function of potential from previous iteration.

The coefficient matrices b, k are formed based on the material of the current node i.e., (i, j). If it is laplace equation, the charge density is taken as zero and hence k is 0. If it is conducting region, b is taken as 1 and k is taken as 0 so as to fill the matrix without any discontinuities.The table 2.1 consists of the coefficients a, b, c, d, e, k for all types of regions we process.

More details on the derivation were given in A.3

Table 2.1: Coefficients of Poisson/Laplace equation

Coefficient	Conductor	Semiconductor	Insulator
a	0	1	1
b	1	$(-4-\frac{qh^2n_i}{\epsilon V_t}(e^{-V(i,j)}+e^{V(i,j)}))$	-4
c	0	1	1
d	0	1	1
e	0	1	1
k	0	$\frac{-qh^2}{\epsilon V_t}(n_ie^{-V(i,j)} - n_ie^{V(i,j)} + N_D(i,j) - N_A(i,j))$+ 4V(i,j)-V(i-1,j)-V(i+1,j)-V(i,j-1)-V(i,j+1)	4V(i,j)-V(i-1,j)-V(i+1,j)-V(i,j-1)-V(i,j+1)

2.3.4. Boundary conditions:

While simulating any rectangular region, we will come across the situation of boundary condition which are the limits for any structure.

For solving the structure, Neumann boundary condition is taken. Example,

$$\begin{aligned} V(i+1,j) &= V(i-1,j) \\ \delta(i+1,j) &= \delta(i-1,j) \end{aligned} \tag{2.14}$$

when i exceeds number of horizontal nodes [13]. Likewise, we have total 8 boundary conditions to implement with 4 being the corners of the structure and remaining are the sides of the structure. The complete boundary conditions for calculating V and δ are shown in Figure 2.4.

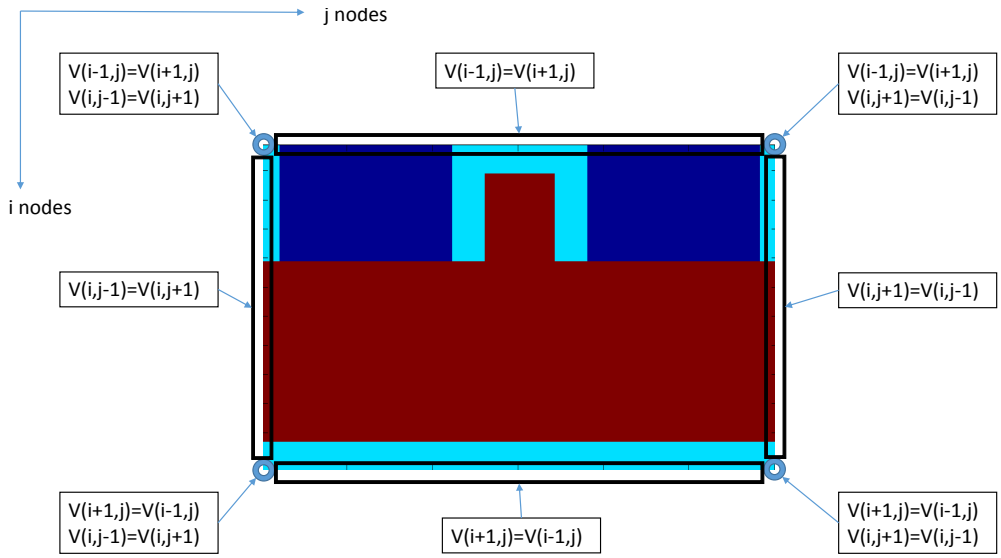

Figure 2.4: Boundary conditions used for calculating potential

2.3.5. Conversion from 2 Dimensional(2D) matrices to 1D matrices:

To solve the equation of the form (3.12), **Matrix inversion method** has been used. Writing equation for each node, we get $m \times n$ number of equations where m is the number of nodes in X direction and n is the number of nodes in Y direction. Solving these equations in their original form requires 3D matrix formulation. To avoid that, the 2D coefficient matrices a, b, c, d, e, k have been converted into 1D by assigning a unique ID, l for each 2D node (i, j). l can be obtained as,

$$l = (number\ of\ horizontal\ nodes)(i-1) + j$$

The scanning of nodes follows horizontal direction as shown in below figure for an example containing 11 nodes in X direction.

Following this, the coefficients a, b, c, d, e have been calculated in 1D and matrix A is formulated. Matrix k is calculated in 1D to formulate matrix B. Then δ can be obtained as, $\delta = A^{-1}B$.

The size of matrix A is $mn \times mn$, which is huge and the program may run out of memory. Hence memory optimization techniques have been implemented for this purpose.

Instead of creating the 2D matrix A, it has been created as a sparse matrix by considering 3 linear arrays. In one array, the x location is stored . Similarly, second array

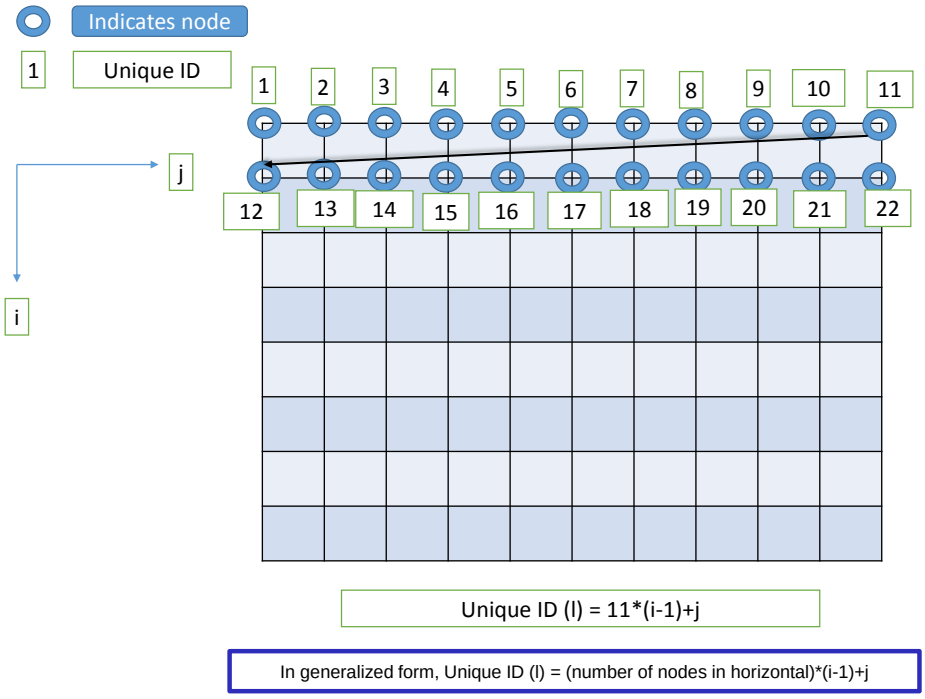

Figure 2.5: Converting 2D to 1D matrix using unique ID

consists of y location and in the final matrix, the corresponding coefficient is stored by using the following transformations.

Since a(i,j) is the coefficient of V(i-1,j) - the upper node,

$$A(l, l-(nodes\ in\ horizontal)) <-- a(i,j) \tag{2.15}$$

$$A(l, l) <-- b(i,j) \tag{2.16}$$

Since c(i,j) is the coefficient of V(i+1,j) - the lower node,

$$A(l, l+(nodes\ in\ horizontal)) <-- c(i,j) \tag{2.17}$$

Since d(i,j) is the coefficient of (i,j-1) - the left node,

$$A(l, l-1) <-- d(i,j) \tag{2.18}$$

Since e(i,j) is the coefficient of (i,j+1) - the right node,

$$A(l, l+1) <-- e(i,j) \tag{2.19}$$

B, X are made single dimension matrices.

$$B(l) <-- k(i,j) \tag{2.20}$$

$$X(l) <-- \delta(i,j) \tag{2.21}$$

2.3.6. Updating the potential and calculating the norm of δ:

The obtained result from matrix inversion method is used to update the potential V by using the following relation which converts back 2D node voltage from 1D using the unique ID relation.

$$V(i,j) = V(i,j) + X(number\ of\ horizontal\ nodes) * (i-1) + j) \tag{2.22}$$

We calculate the norm of the matrix X and if it is less than tolerance value which is 1×10^{-5} normalized volts, we consider the current potential distribution as the solution of the Poisson equation.
And by using the Boltzmann equations , the electron and hole concentrations were obtained. The potential distribution is shown in the Figure 3.1.

2.4 Optical characteristics at equilibrium -Eigen mode equation

Before fabricating the waveguide, we need to know the Mode profile, effective index,absorption coefficient and related information to explain the optical characteristics of that opto-electronic device. In this section, the discretized wave equations were discussed.

The non-magnetic medium with the relative permittivity ϵ_r, the vectorial wave equation for electric field **E** is,

$$\nabla^2\mathbf{E} + \nabla(\frac{\nabla\epsilon_r}{\epsilon_r}.\mathbf{E}) + k_0^2\epsilon_r\mathbf{E} = 0 \tag{2.23}$$

where ∇^2 is laplacian operator andd can be represented as $\frac{\partial^2}{\partial x^2} + \frac{\partial^2}{\partial y^2} + \frac{\partial^2}{\partial z^2}$.
$\nabla\epsilon$ indicates the dielectric constant variation along X and Y directions.
k_0 is the wave number in free space. $k_0 = \omega\sqrt{\mu_0\epsilon_0}$
Similarly for magnetic field,

$$\nabla^2\mathbf{H} + \frac{\nabla\epsilon_r}{\epsilon_r} \times (\nabla \times \mathbf{H}) + k_0^2\epsilon_r\mathbf{H} = 0 \tag{2.24}$$

ϵ_r is assumed to be independent of z direction.

the above equations can be modified as below if the cross components were neglected which are usually small leading to semivectorial equations and can be solved numerically.

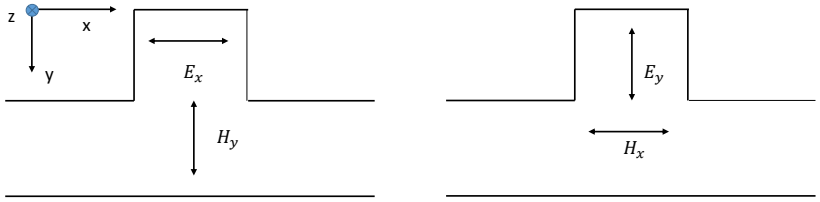

Figure 2.6: The field components for Quasi TE and TM ploarizations

Furthermore, These equations can be analyzed considering quasi TE or quasi TM modes which have E_x and H_y or E_y and H_x as their field components respectively [10].

If we consider $\frac{\partial}{\partial z} = -j\beta$, TE wave equation can be written as,

$$\frac{\partial}{\partial x}\big(\frac{1}{\epsilon_r}\frac{\partial}{\partial x}(\epsilon_r E_x)\big) + \frac{\partial^2 E_x}{\partial y^2} + (k_0^2\epsilon_r - \beta^2)E_x = 0 \tag{2.25}$$

and TM wave equation is,

$$\frac{\partial^2 E_y}{\partial x^2} + \frac{\partial}{\partial y}(\frac{1}{\epsilon_r}\frac{\partial}{\partial y}(\epsilon_r E_y)) + (k_0^2\epsilon_r - \beta^2)E_y = 0 \tag{2.26}$$

Considering TE wave equations,using the finite difference scheme assuming uni-

form mesh size throughout the structure. If we consider that (i,j) as the node that represents the point of the region at a distance of $i \times h$ horizontal direction and $j \times h$ from vertical direction , these can be rewritten as,

$$\begin{aligned} \frac{\partial^2 E_x}{\partial x^2} &= \frac{E(i+1,j) + E(i-1,j) - 2E(i,j)}{h^2} \\ \frac{\partial^2 E_x}{\partial y^2} &= \frac{E(i,j+1) + E(i,j-1) - 2E(i,j)}{h^2} \end{aligned} \tag{2.27}$$

The above equation can be written of the form,

$$AE(i+1,j)+BE(i-1,j)+CE(i,j+1)+DE(i,j-1)+FE(i,j) = GE(i,j) \tag{2.28}$$

where A, B, C, D, F, G are the coefficients explained above for both TE and TM polarizations. The standard derivation of eigen mode equations and related approximations were discussed in detail in appendix A.2.

The equations are solved for Quasi TE and TM modes. These equations are known as, semivectorial wave equations since, the coupled field components are neglected.

Table 2.2: Coefficients of eigen mode equations

	TE Polarization	**TM Polarization**
A	$\frac{2\epsilon_r(i+1,j)}{\epsilon(i+1,j)+\epsilon(i,j)} \frac{1}{(k_0 \times h)^2}$	$\frac{1}{(k_0 \times h)^2}$
B	$\frac{2\epsilon_r(i-1,j)}{\epsilon(i-1,j)+\epsilon(i,j)} \frac{1}{(k_0 \times h)^2}$	$\frac{1}{(k_0 \times h)^2}$
C	$\frac{1}{(k_0 \times h)^2}$	$\frac{2\epsilon_r(i,j+1)}{\epsilon(i,j+1)+\epsilon(i,j)} \frac{1}{(k_0 \times h)^2}$
D	$\frac{1}{(k_0 \times h)^2}$	$\frac{2\epsilon_r(i,j-1)}{\epsilon(i,j-1)+\epsilon(i,j)} \frac{1}{(k_0 \times h)^2}$
F	ϵ_r(i,j)- 2(1+ϵ_r(i,j))($\frac{1}{\epsilon_r(i+1,j)+\epsilon_r(i,j)}$ + $\frac{1}{\epsilon_r(i-1,j)+\epsilon_r(i,j)}$)	$\epsilon_r(i,j)$ − 2(1 + $\epsilon_r(i,j)$)($\frac{1}{\epsilon_r(i+1,j)+\epsilon_r(i,j)}$ + $\frac{1}{\epsilon_r(i-1,j)+\epsilon_r(i,j)}$)
G	$\beta^2/k_0^2 = n_{eff}^2$	$\beta^2/k_0^2 = n_{eff}^2$

From equations (1.3) and (1.4) , the change in refractive index (Δn) and change in absorption coefficient ($\Delta\alpha$) can be obtained from change in electron and hole concentrations.

The discretized equations mentioned above were solved and the optical characteristics mainly Effective index(n_{eff}), absorption coefficient(α_{eff}), Mode profile were obtained for both quasi TE and TM polarizations. The mode profiles were shown in figure 3.2.

The program code is developed by IOLAB [15] and the code has been adapted and modified so as to meet the requirements of this algorithm mainly, the plasma dispersion effect as explained through equations 1.3 and 1.4.

2.5 Steady state electrical and optical characteristics at forward bias

In equilibrium, since the drift is balanced by diffusion for both electrons and holes, there will be no carrier movement. Hence, transport and continuity equations were not solved. In applied bias condition, the poisson equation need to be solved along with continuity and transport equations. The procedure is explained below.

2.5.1. Increase the voltage at anode:

The anode voltage i.e., the potential at the surface of the conductor is increased in multiple of step voltage as mentioned at the starting of the program.

2.5.2. Solving the drift-diffusion equation:

Conduction in a semiconductor will happen through Drift (which is due to presence of electric field) and Diffusion (which happens because of concentration gradient). Including both these effects, the current densities for electrons and holes can be written in 1D as,

$$\boxed{\begin{aligned} J_p(x) &= q\mu_p(x)p(x)E(x) - qD_p(x)\frac{dp(x)}{dx} \\ J_n(x) &= q\mu_n(x)n(x)E(x) + qD_n(x)\frac{dn(x)}{dx} \end{aligned}} \tag{2.29}$$

where q is electron charge and is = 1.6 $\times 10^{-19}$ $Coloumb$. J_p, J_n are the current density of hole and electron respectively. μ_p, μ_n are the mobility of hole and electron. E is the electric field. p, n are the hole and electron concentrations. x is the distance from anode. D_p, D_n are the diffusion constants and can be related to mobility with following Einstein relation.

$$\begin{aligned} D_p &= \mu_p \times V_t \\ D_n &= \mu_n \times V_t \end{aligned} \tag{2.30}$$

where V_t is the thermal voltage and = $kT/q = 0.026eV$ at room temperature.

The total current density

$$J(x) = J_p(x) + J_n(x) \tag{2.31}$$

The above mentioned are Transport equations. Electron and hole concentrations vary with distance x and tend to recombine. This can be explained with continuity equation which states that,

Rate of carrier buildup = Net generation rate - Net rate of carriers leaving

Writing in derivative form,

$$\boxed{\begin{aligned} \frac{\partial p}{\partial t} &= g - \frac{1}{q}\frac{\partial J_p}{\partial x} \\ \frac{\partial n}{\partial t} &= g + \frac{1}{q}\frac{\partial J_n}{\partial x} \end{aligned}} \tag{2.32}$$

where $g = -U$ is the generation-recombination rate of carriers which is already discussed in the previous chapter.

In order to process the equations for simulation, they need to be discretized. Considering the transport equation,

$J_p(x) = q\mu_p(x)p(x)E(x) - qD_p(x)\frac{dp(x)}{dx}$

If we assume that current density J_p, electric field E, mobility μ_p are assumed to be constant within the node as shown in Figure 2.7, we can rewrite the equation as,

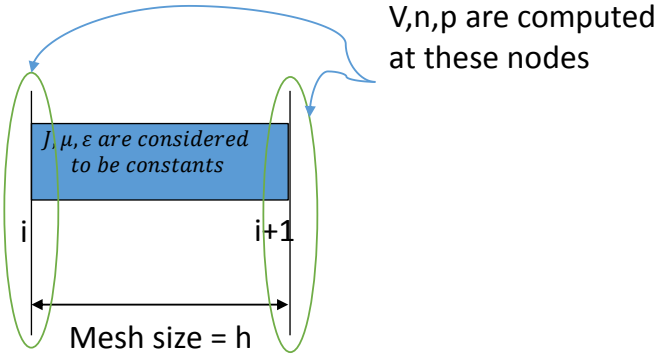

Figure 2.7: Scharfetter-Gummel Discretization scheme

$$=> qD_p \frac{dp(x)}{dx} = q\mu_p p(x)E - J_p$$

$$=> \frac{dp(x)}{q\mu_p p(x)E - J_p} = \frac{dx}{qD_p}$$

$$=> \int_{p(i)}^{p(i+1)} \frac{dp(x)}{q\mu_p p(x)E - J_p} = \int_{ih}^{(i+1)h} \frac{dx}{qD_p}$$

By solving this with help of equation 2.30, we get the equation of the form,

$$J_p\left(e^{Eh/V_t} - 1\right) = -q\mu_p p(i+1)E + q\mu_p p(i)Ee^{Eh/V_t} \tag{2.33}$$

where E is the electric field which is constant within the cell and can be written as ,

$$\begin{aligned} E = -\frac{dV}{dx} &= -\frac{V(i+1) - V(i)}{h} \\ &= \frac{V(i) - V(i+1)}{h} \end{aligned} \tag{2.34}$$

From equations 2.33 and 2.34, we get [12]

$$J_p(i+1/2) = \left[-p(i+1)B\left(\frac{V(i)}{V_t} - \frac{V(i+1)}{V_t}\right) + p(i)B\left(\frac{V(i+1)}{V_t} - \frac{V(i)}{V_t}\right)\right] \times \frac{qD_p(i+1/2)}{h} \tag{2.35}$$

Similarly for electron, we get

$$J_n(i+1/2) = \left[n(i+1)B\left(\frac{V(i+1)}{V_t} - \frac{V(i)}{V_t}\right) - n(i)B\left(\frac{V(i)}{V_t} - \frac{V(i+1)}{V_t}\right)\right] \times \frac{qD_n(i+1/2)}{h} \tag{2.36}$$

where

$$B(x) = \frac{x}{e^x - 1} \tag{2.37}$$

Equation 2.32 can be discretized as,

$$\frac{p_i^{(k+1)} - p_i^{(k)}}{\Delta t} = g - \frac{1}{qh}(J_p(i+1/2) - J_p(i-1/2)) \tag{2.38}$$

where k indicates $k \times \Delta t$ time.

From equations 2.35 and 2.38 we get,

$$\boxed{\begin{aligned} -g + \frac{p^{(k+1)}(i) - p^{(k)}(i)}{\Delta t} = \frac{1}{qh^2}\Bigg[& p(i-1)D_p(i-1/2)B\big(\frac{V(i)}{V_t} - \frac{V(i-1)}{V_t}\big) \\ -p(i)\big(D_p(i+1/2)B\big(\frac{V(i+1)}{V_t} - \frac{V(i)}{V_t}\big) & + D_p(i-1/2)B\big(\frac{V(i-1)}{V_t} - \frac{V(i)}{V_t}\big) \\ & + p(i+1)D_p(i+1/2)B\big(\frac{V(i)}{V_t} - \frac{V(i+1)}{V_t}\big)\Bigg] \end{aligned}} \tag{2.39}$$

Similarly for electron,

$$-g+\frac{n^{(k+1)}(i)-n^{(k)}(i)}{\Delta t}=\frac{1}{qh^2}\Bigg[n(i-1)D_n(i-1/2)B\big(\frac{V(i-1)}{V_t}-\frac{V(i)}{V_t}\big)$$
$$-n(i)\big(D_n(i-1/2)B\big(\frac{V(i)}{V_t}-\frac{V(i-1)}{V_t}\big)+D_n(i+1/2)B\big(\frac{V(i)}{V_t}-\frac{V(i+1)}{V_t}\big)$$
$$+n(i+1)D_n(i+1/2)B\big(\frac{V(i+1)}{V_t}-\frac{V(i)}{V_t}\big)\Bigg] \tag{2.40}$$

After increasing the voltage at the electrode, this drift-diffusion equation is solved in order to obtain the modified electron and hole concentrations. This equation is solved **only for semiconductor region** since there will be no current flow inside insulator. The equations 2.39 and 2.40 can be extended to 2D as,

$$U(i,j)=\frac{1}{qh^2}\Bigg[p(i-1,j)D_p(i-1/2,j)B\big(\frac{V(i,j)}{V_t}-\frac{V(i-1,j)}{V_t}\big)$$
$$-p(i,j)\big(D_p(i+1/2,j)B\big(\frac{V(i+1,j)}{V_t}-\frac{V(i,j)}{V_t}\big)+$$
$$D_p(i-1/2,j)B\big(\frac{V(i-1,j)}{V_t}-\frac{V(i,j)}{V_t}\big)$$
$$+D_p(i,j-1/2)B\big(\frac{V(i,j-1)}{V_t}-\frac{V(i,j)}{V_t}\big)+D_p(i,j+1/2)B\big(\frac{V(i,j+1)}{V_t}-\frac{V(i,j)}{V_t}\big)$$
$$+p(i+1,j)D_p(i+1/2,j)B\big(\frac{V(i,j)}{V_t}-\frac{V(i+1,j)}{V_t}\big)$$
$$+p(i,j-1)D_p(i,j-1/2)B\big(\frac{V(i,j)}{V_t}-\frac{V(i,j-1)}{V_t}\big)$$
$$+p(i,j+1)D_p(i,j+1/2)B\big(\frac{V(i,j)}{V_t}-\frac{V(i,j+1)}{V_t}\big)\Bigg] \tag{2.41}$$

Similarly for electron,

$$\begin{aligned}
U(i,j) = \frac{1}{qh^2}\Big[& n(i-1,j)D_n(i-1/2,j)B\big(\frac{V(i-1,j)}{V_t} - \frac{V(i,j)}{V_t}\big) \\
& -n(i,j)\big(D_n(i+1/2,j)B\big(\frac{V(i,j)}{V_t} - \frac{V(i+1,j)}{V_t}\big)+ \\
& D_n(i-1/2,j)B\big(\frac{V(i,j)}{V_t} - \frac{V(i-1,j)}{V_t}\big) \\
& +D_n(i,j-1/2)B\big(\frac{V(i,j)}{V_t} - \frac{V(i,j-1)}{V_t}\big) + D_n(i,j+1/2)B\big(\frac{V(i,j)}{V_t} - \frac{V(i,j+1)}{V_t}\big) \\
& +n(i+1,j)D_n(i+1/2,j)B\big(\frac{V(i+1,j)}{V_t} - \frac{V(i,j)}{V_t}\big) \\
& +n(i,j-1)D_n(i,j-1/2)B\big(\frac{V(i,j-1)}{V_t} - \frac{V(i,j)}{V_t}\big) \\
& +n(i,j+1)D_n(i,j+1/2)B\big(\frac{V(i,j+1)}{V_t} - \frac{V(i,j)}{V_t}\big)\Big]
\end{aligned} \tag{2.42}$$

where (i,j) indicates the current node. The voltage distribution of the previous step is taken as initial guess and the concentrations at conductor-semiconductor boundary as considered to be constant and equal to the equilibrium concentrations. The diffusitivity constants D_p, D_n can be obtained from equation 2.30 and U is obtained from Recombination theory explained in previous chapter.

Initially $U(i,j)$ is considered as zero.

2.5.3. Boundary conditions:

The above equations can be written of the form,

$$\begin{aligned}
& a(i,j)p(i-1,j) + b(i,j)p(i,j) + c(i,j)p(i+1,j) \\
& +d(i,j)p(i,j-1) + e(i,j)p(i,j+1) = U(i,j)
\end{aligned} \tag{2.43}$$

where a, b, c, d, e are the coefficients which are function of normalized potential and mobility. The boundary conditions for above equations are shown in the Figure 2.8.

At the semiconductor-insulator junction, neumann boundary conditions were used and at conducting boundary, dirichlet boundary conditions were used since the carrier concentration at conductor-semiconductor junction is same as equilibrium concentra-

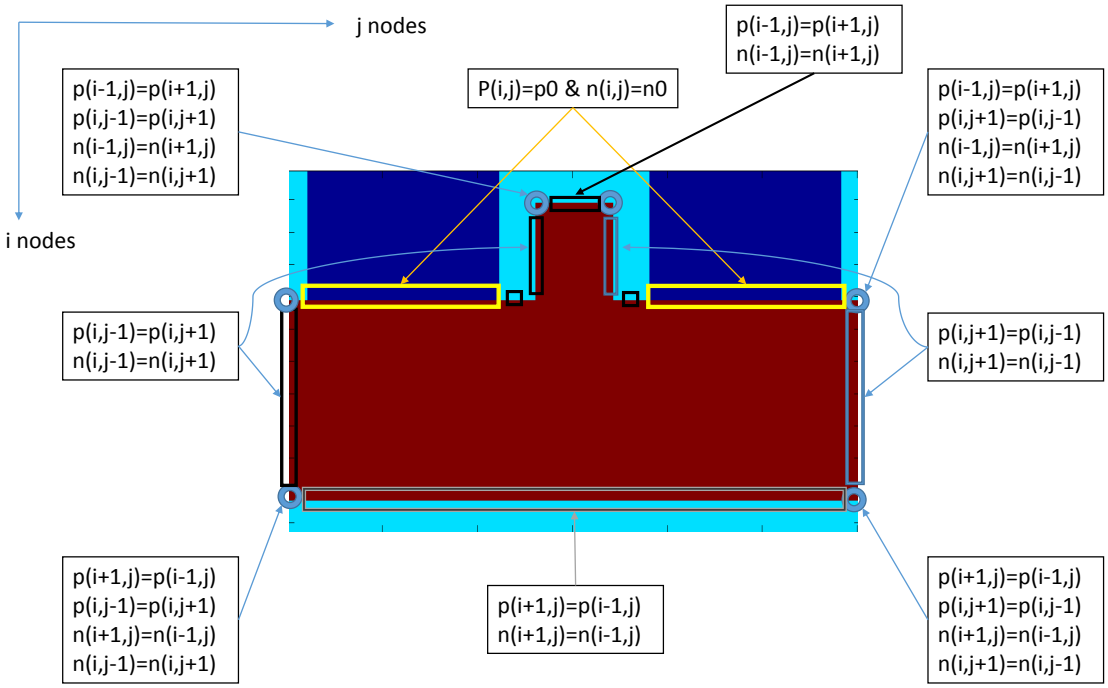

Figure 2.8: Boundary conditions used for calculating carrier concentrations

tion because of infinite amount of recombinations at the surfaces.

As per the boundary conditions, the matrices a, b, c, d, e were formulated with U being the recombination coefficient.

For a node which is below conductor-semiconductor junction, the equation can be written as,

$$\begin{aligned} b(i,j)p(i,j) + c(i,j)p(i+1,j) + d(i,j)p(i,j-1) \\ +e(i,j)p(i,j+1) = U(i,j) - a(i,j)p_0(i-1,j) \end{aligned} \tag{2.44}$$

where p_0 denotes the equilibrium hole concentration.

2.5.4. Converting from 2D matrices to 1D matrices:

To solve these equations, the carrier concentrations are converted from 2D to 1D using unique ID as explained in section 2.3 while solving for equilibrium.

2.5.5. Rewriting the carrier concentrations and Generation-Recombination rate:

With Matrix inversion method, the carrier concentrations were calculated and the 2D carrier concentration were replaced with new values using the unique ID. With the modified carrier concentrations, the generation-recombination rate $U(i,j)$ will be updated [13].

2.5.6. Solving the linearized Poisson equation:

With the carrier concentrations obtained above, we solve for Poisson equation. Since, the fermilevel is changed after positive bias, the equilibrium procedure for poisson equation is not considered.

The Poisson equation is solved for **potential** for the complete region. The equation (2.17) can be written as,

$$\begin{aligned} &\delta(i+1,j)+\delta(i-1,j)+\delta(i,j-1)+\delta(i,j+1)+ \\ &\qquad \delta(i,j)\left(-4-\frac{qh^2}{\epsilon V_t}(p(i,j)+n(i,j))\right) \\ &=4V(i,j)-V(i+1,j)-V(i-1,j)-V(i,j-1)-V(i,j+1)- \\ &\qquad \frac{qh^2}{\epsilon V_t}\Big(p(i,j)-n(i,j)+N_D(i,j)-N_A(i,j)\Big) \end{aligned} \tag{2.45}$$

The above equation is of the form (2.13) and the coefficients can be found in similar way mentioned in section (2.2.3).

2.5.7. Boundary conditions:

The procedure mentioned in section (2.2.4) was repeated for boundary conditions for calculating the potential.

2.5.8. Conversion from 2D matrices to 1D matrices:

For updating the potential,the linearization principle used in section (2.2.5) was used here.

2.5.9. Updating the potential and calculating the norm of δ:

After formulating the equation(2.51) to AX=B form, X or δ is calculated with matrix inversion method. After calculating X , the potential V is updated by using the following relation.

$$V(i,j) = V(i,j) + \delta(number\ of\ horizontal\ nodes) * (i-1) + j) \tag{2.46}$$

The norm of the matrix X is calculated and if it is less than tolerance value, we consider the current electrical characteristics as the solution for the region and we exit from the iteration. Potential distribution is shown in 3.3 and recombination coefficient is shown in 3.5.

2.5.10. Calculating Current density:

After obtaining the potential and concentrations from above step, the current densities are back calculated using equations 2.35 and 2.36 for all nodes in the **semiconductor region** only. The current density is shown in Figure 3.4.

2.5.11. Optical characteristics:

The method explained in section (2.4) for calculating the Field profile, effective index and absorption coefficients for applied bias is applied for steady state. The mode profiles for TE and TM polarizations were shown in Figure 3.7.

2.5.12. Incrementing the step voltage:

The step voltage is given at the start of the simulation. In this step, we check if the anode voltage exceeding the applied voltage. If it does, we will end the steady state analysis. Otherwise, we increment the voltage at anode to next multiple of the step voltage and begin from step 1.

The results are shown in next chapter are for applied bias of 1 volt.

The applied voltage is extended more than 1 volt and plotted the variation of current density J at mid point of the rib structure and the current density variation with respect to applied anode voltage is shown in Figure 3.6.

2.6 Transient characteristics

We tried to analyze the transient characteristics of the structure for an AC small signal voltage and the results are hopefully positive and can be improved by adapting and investigating various time domain techniques for calculating the rise time , fall time and bandwidth. Below is the procedure to calculate the transient parameters.

For calculating the transient characteristics the equations can be written for node (i, j) as [14],

$$U(i,j)\Big]_k + \frac{p^{(k+1)}(i,j) - p^{(k)}(i,j)}{\Delta t} = \frac{1}{qh^2}\Bigg[p(i-1,j)D_p(i-1/2,j)B\big(\frac{V(i,j)}{V_t} - \frac{V(i-1,j)}{V_t}\big)$$
$$-p(i,j)\big(D_p(i+1/2,j)B\big(\frac{V(i+1,j)}{V_t} - \frac{V(i,j)}{V_t}\big)+$$
$$D_p(i-1/2,j)B\big(\frac{V(i-1,j)}{V_t} - \frac{V(i,j)}{V_t}\big)$$
$$+D_p(i,j-1/2)B\big(\frac{V(i,j-1)}{V_t} - \frac{V(i,j)}{V_t}\big) + D_p(i,j+1/2)B\big(\frac{V(i,j+1)}{V_t} - \frac{V(i,j)}{V_t}\big)$$
$$+p(i+1,j)D_p(i+1/2,j)B\big(\frac{V(i,j)}{V_t} - \frac{V(i+1,j)}{V_t}\big)$$
$$+p(i,j-1)D_p(i,j-1/2)B\big(\frac{V(i,j)}{V_t} - \frac{V(i,j-1)}{V_t}\big)$$
$$+p(i,j+1)D_p(i,j+1/2)B\big(\frac{V(i,j)}{V_t} - \frac{V(i,j+1)}{V_t}\big)\Bigg]_{(k+1)} \tag{2.47}$$

Similarly for electron,

$$U(i,j)\Big]_k + \frac{n^{(k+1)}(i,j) - n^{(k)}(i,j)}{\Delta t} = \frac{1}{qh^2}\Bigg[n(i-1,j)D_n(i-1/2,j)B\big(\frac{V(i-1,j)}{V_t} - \frac{V(i,j)}{V_t}\big)$$
$$-n(i,j)\big(D_n(i+1/2,j)B\big(\frac{V(i,j)}{V_t} - \frac{V(i+1,j)}{V_t}\big)+$$
$$D_n(i-1/2,j)B\big(\frac{V(i,j)}{V_t} - \frac{V(i-1,j)}{V_t}\big)$$
$$+D_n(i,j-1/2)B\big(\frac{V(i,j)}{V_t} - \frac{V(i,j-1)}{V_t}\big) + D_n(i,j+1/2)B\big(\frac{V(i,j)}{V_t} - \frac{V(i,j+1)}{V_t}\big)$$
$$+n(i+1,j)D_n(i+1/2,j)B\big(\frac{V(i+1,j)}{V_t} - \frac{V(i,j)}{V_t}\big)$$
$$+n(i,j-1)D_n(i,j-1/2)B\big(\frac{V(i,j-1)}{V_t} - \frac{V(i,j)}{V_t}\big)$$
$$+n(i,j+1)D_n(i,j+1/2)B\big(\frac{V(i,j+1)}{V_t} - \frac{V(i,j)}{V_t}\big)\Bigg]_{(k+1)} \tag{2.48}$$

2.6.1. Fixing the dc bias point

Before proceeding to transient analysis, a dc bias point should be fixed on which AC small signal voltage need to be applied. For this case, 1 volt has been chosen to be the bias point.

2.6.2. Applying the AC signal

The AC signal was taken to be 0.01 V(peak-to-peak) amplitude which is 1% of the dc bias voltage.

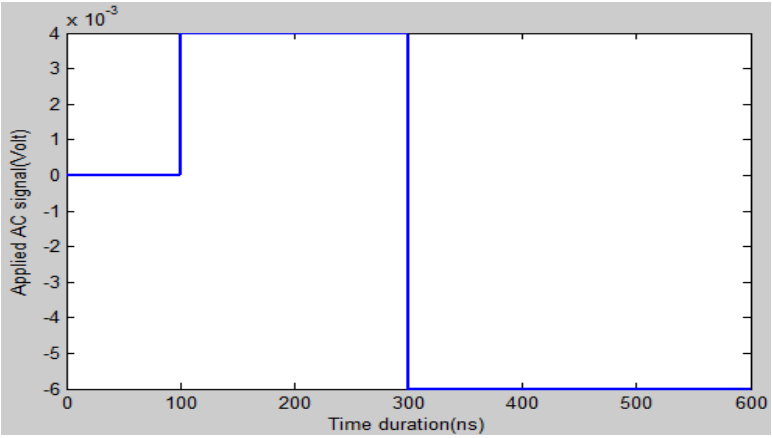

Figure 2.9: Input AC signal

2.6.3. Starting the iterative procedure and Choosing the time step Δt

Time step is limited by dielectric relaxation time. It is defined as the time at which the charge density inside a volume reduces to 1/e of it's initial value. And is the quantity which indicates the conductivity of the material.

$$t_{dr} = \frac{\epsilon}{qN\mu} \tag{2.49}$$

where ϵ is the dielectric constant of the material. q denotes the charge, N is the doping concentration and μ denotes the mobility of the charge carrier. The step size should be atleast one tenth of t_{dr} [13].

For this case, since the time step is of femto seconds, adaptive time step technique is considered. At voltage step increase, more number of samples are taken and at remaining voltage levels, less number of samples were considered by increasing the step size. For above input, at the rising edge till another 2ns and at the falling edge till another 2ns, time step of $10^{-16} sec$ is taken and the step size decrements as the applied voltage is constant.

2.6.4. Procedure for iteration

U has been updated with carrier concentration using SRH theory.

For each time step, the input voltage is sampled and applied to anode of the device. Followed by the obtaining the solution of above equation followed by the steps mentioned from (2.5.3) till (2.5.11).

This procedure is followed till complete time period is reached. the result is shown in 3.8.

CHAPTER 3

Simulation Results and Discussion

In this chapter, we have shown the results obtained from our simulator and from device simulator MEDICI [16].

3.1 Equilibrium

Electrical and Optical characteristics were shown under zero applied bias.

3.1.1 Electrical characteristics

Equilibrium potential distribution:

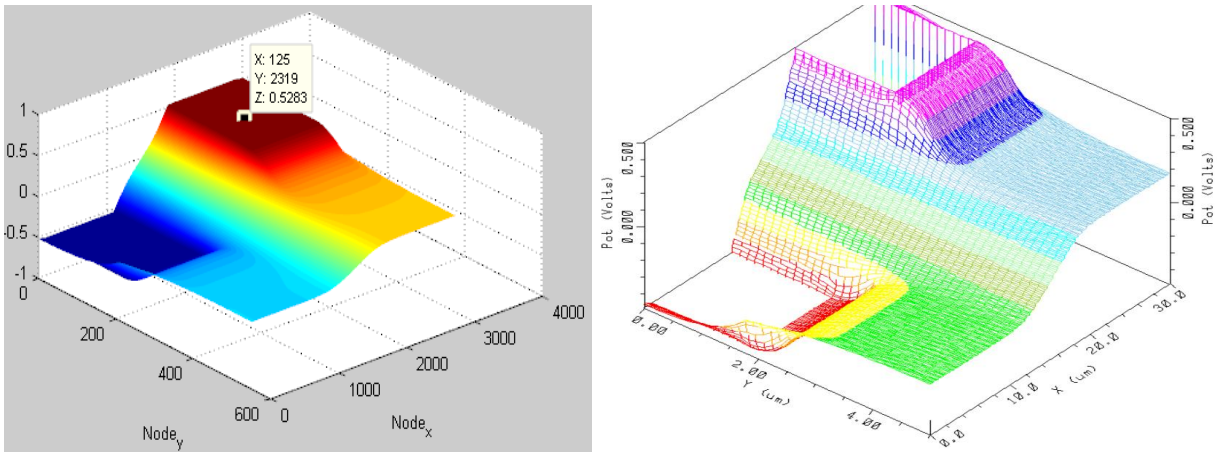

$$\text{Built-in Voltage} = 2 \times 0.026 \times \ln\left(\frac{10^7}{0.015}\right) = 2 \times 0.5282628 = 1.05652\ V$$

Figure 3.1: Equilibrium potential distribution

The potential we obtained from the simulation is in accordance with the theoretical result. The second figure is the voltage distribution obtained from medici. The tendency of the results are matching though, some variation is observed because of boltzmann approximation and neglecting heavy doping effects on intrinsic carrier concentration.

3.1.2 Optical characteristics

Field Profile:

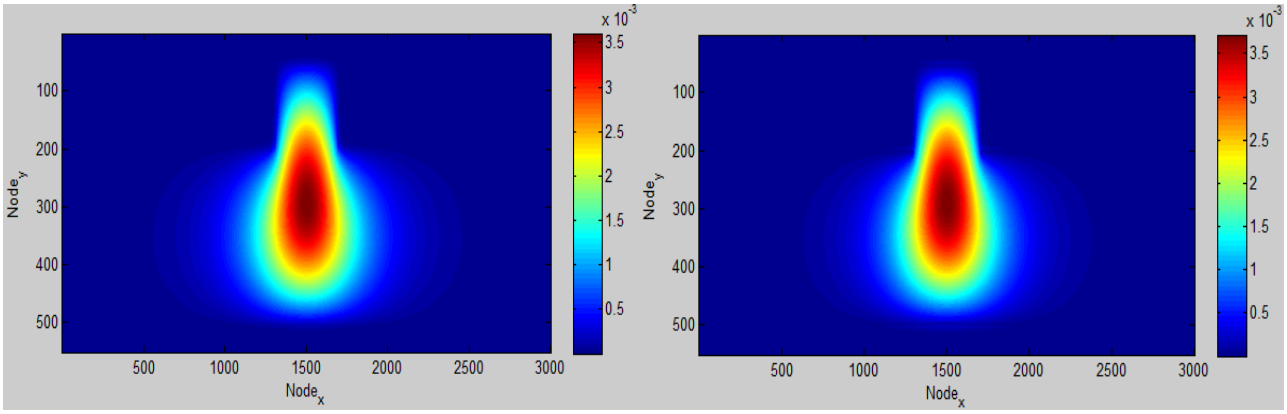

Figure 3.2: TE and TM mode profile at equilibrium

3.2 Steady state forward bias

Electrical and Optical characteristics were shown under forward bias of 1volt.

3.2.1 Electrical characteristics

Potential distribution:

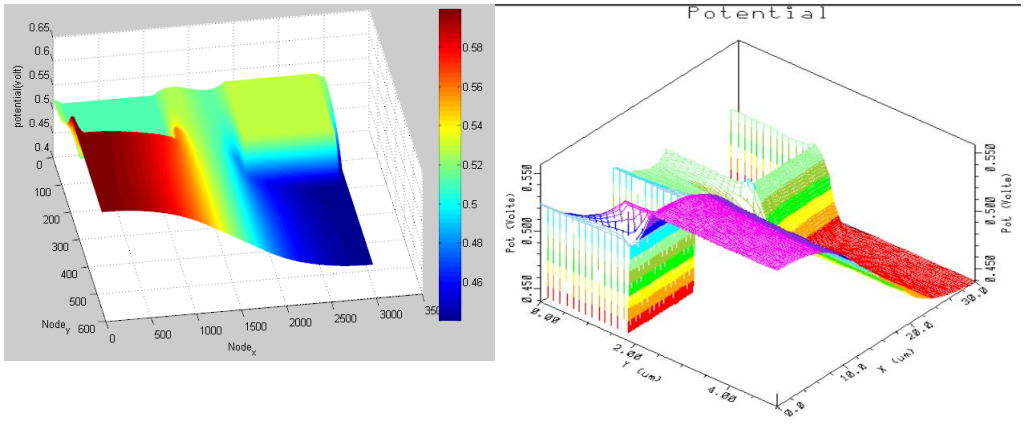

Figure 3.3: Potential distribution at applied bias. Left figure is the result obtained from the program. The right figure shows the result calculating from medici.

Since, the mobility depends only on impurity concentration and Auger recombination is neglected, the variation is observed. However, the results are in agreement with the expected variation.

Current density distribution:

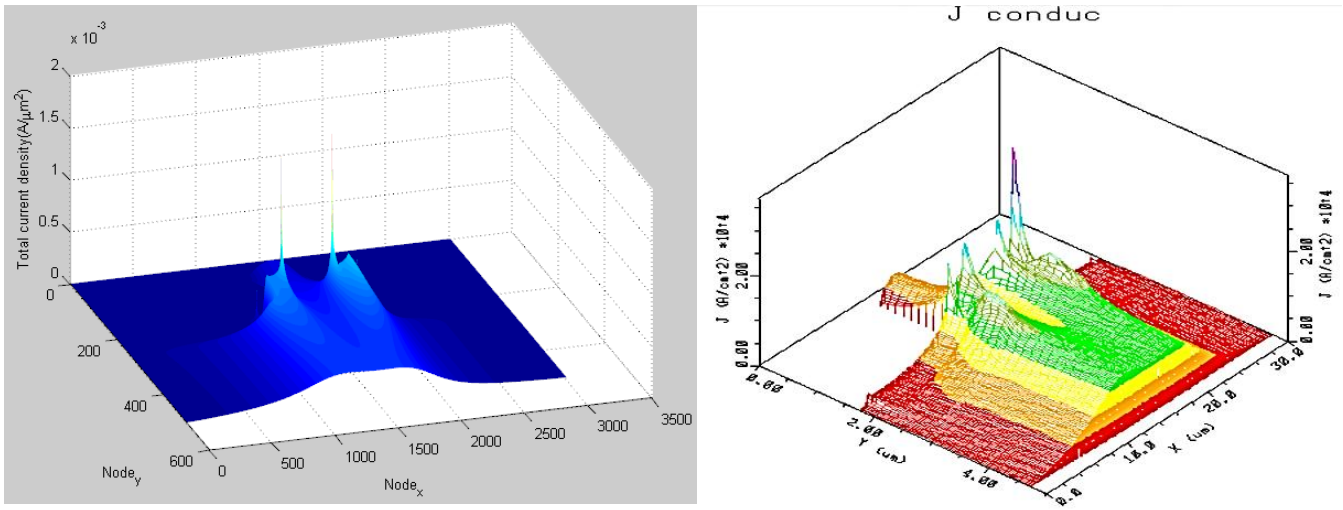

Figure 3.4: Current density distribution at applied bias of 1 Volt. The right figure shows the result obtained from medici. The peaks are observed some nodes in the region because of the reason that the lateral electrodes were considered.

Recombination coefficient:

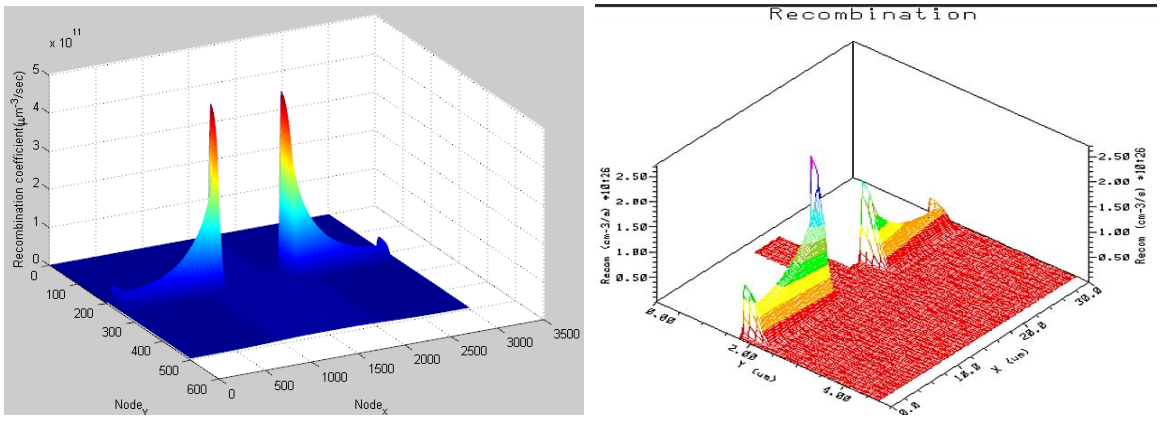

Figure 3.5: Recombination coefficient at applied bias

Since, Auger recombination is neglected and the recombination model is symmetric for P and N type semiconductors, the program result shows symmetry and hence the

variation occurred comparing with medici result.

I-V characteristics:

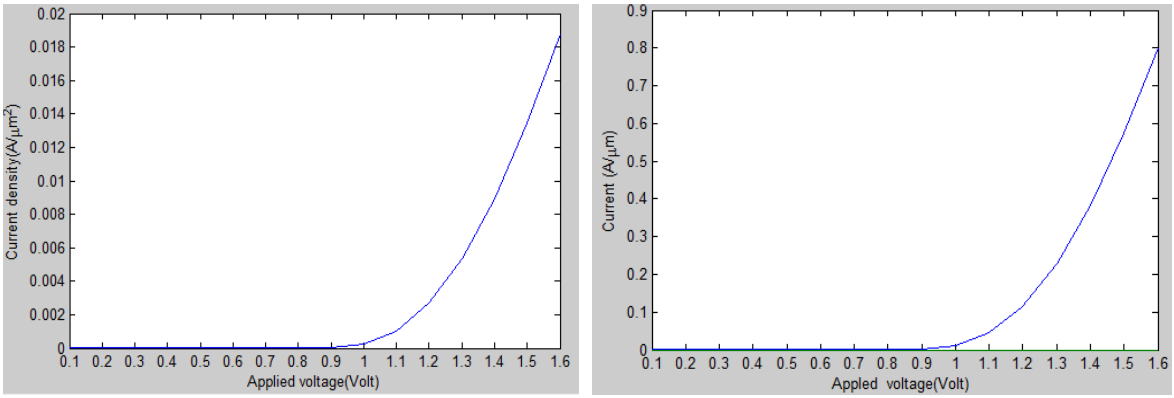

Figure 3.6: Current density-Voltage forward bias characteristics are shown. The left plot shows the variation of current density J at the center of waveguide cross section with applied voltage varied from 0 to 1.6 Volt. The right plot is the current variation with applied voltage.

3.2.2 Optical characteristics

Field Profile:

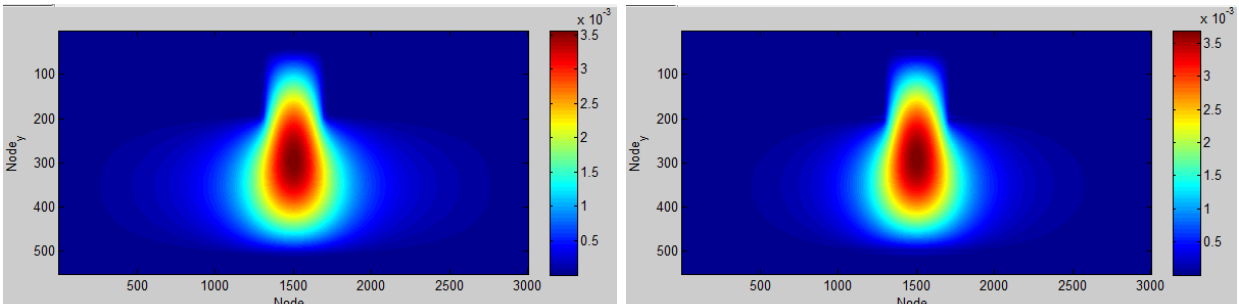

Figure 3.7: TE and TM mode profiles for applied bias of 1 Volt

3.3 Transient characteristics

The transient characteristics were shown which were obtained from adaptive time step technique. It can be further investigated.

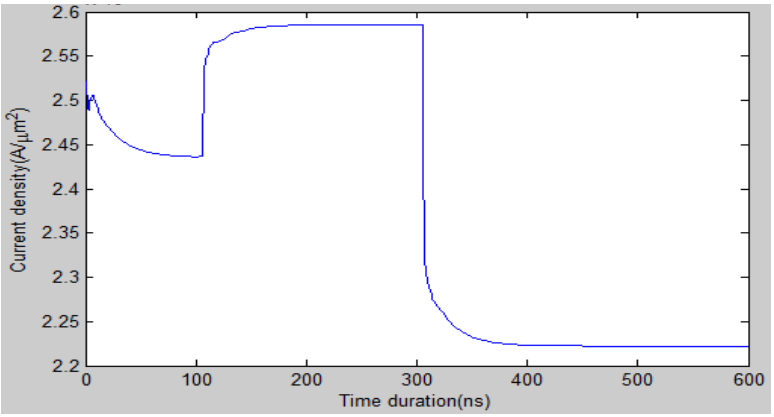

Figure 3.8: Current density variation at the center of waveguide geometry as a function of time with applied AC signal.

3.4 Derived parameters

With the assumptions considered, we have extracted the electro-optic effects in silicon optical modulator and they are close to the practical results obtained.

Built-in potential = V_0 = 1.05 Volt

Total current I = 0.04424 A/μm

n_{eff}^{TE} at equilibrium= 3.47112

n_{eff}^{TM} at equilibrium= 3.47086

n_{eff}^{TE} at applied bias of 1 volt= 3.46817

n_{eff}^{TM} at applied bias of 1 volt=3.4679

L_{π}^{TE} = $\frac{1.55}{2\times(3.47112-3.46817)}$ =262.712μm

L_{π}^{TM} = $\frac{1.55}{2\times(3.47086-3.4679)}$=261.824$\mu$m

Figure of Merit = 0.262712 V-mm or 0.261824 V-mm

3.5 Graphical user interface

Each parameter of the obtained electrical and optical characteristics have been stored in a multidimensional array at equilibrium and at all step voltages. The parameters include:

1)Potential distribution

2)Electron concentration

3)Hole concentration

4)Recombination coefficient

5)Electric field distribution

6)Electron and hole current densities

7)Effective index

8)Mode profile

9)Absorption coefficient

10)Confinement in X and Y directions of the mode

For the structure shown in Figure (3.2), the graphical interface is shown below.

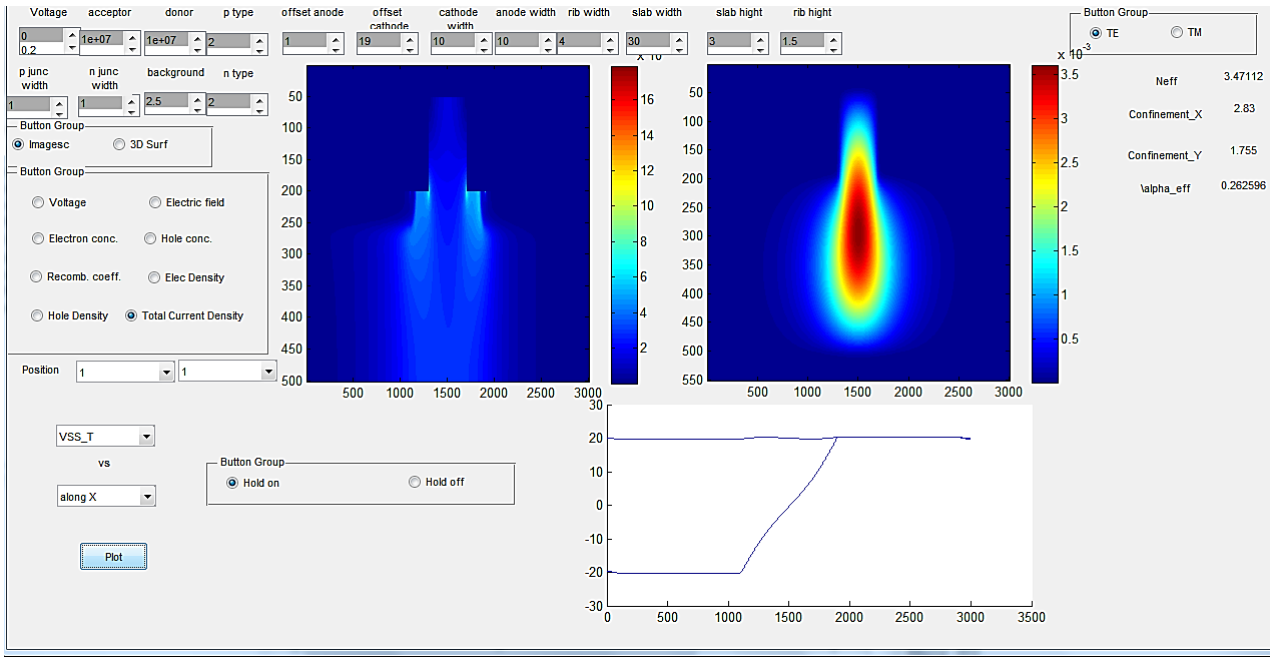

Figure 3.9: Graphical user interface showing the electrical and optical characteristics in separate plots with third figure showing the voltage distribution in 1D along X direction for applied bias and for equilibrium

CHAPTER 4

Conclusions

4.1 Summary

By using the Matlab, with assumptions considered in section 2.2, by considering Large cross section rib waveguide, the electro-optic effects were calibrated and are close to the practical values obtained at our lab. For diffusion type doping with surface concentration of $1 \times 10^{19}\ cm^{-3}$, junction depth of 1 μm and with variation of 1volt, length required for π phase shift is around 250 μm.

The program can process at least one lakh nodes in contrast to most of the simulators which limit the number of nodes. Since finite difference algorithm is used, equal number of nodes will be processed for both electrical and optical characteristics. With graphical user interface, the changes in the output characteristics can be observed with the variation in input parameters such as variation of effective index with junction depth. The memory usage, time consumption are the limitations of the program which can be overcome with optimization techniques.

4.2 Outlook

The project can be extended further. Some of the future work which can be implemented are mentioned below.

4.2.1 Study on transient characteristics

The transient characteristics can be made more accurate by studying various time discretization techniques and applying appropriate one for the semiconductor device simulation.

4.2.2 Generalizing the program

The program has some assumptions based on which it delivers the results we needed. These assumptions can be relaxed so that it furnishes the results which are more closer to practical results.

APPENDIX A

Appendix

A.1 Finite Difference Method

Given a function $f(x)$ we can write its derivative as ,

$$f'(x) = \frac{f(x + \Delta x) - f(x)}{\Delta x} \tag{A.1}$$

assuming Δx to be very small.

The second derivative can be written as,

$$f''(x) = \frac{f(x + \Delta x) - 2f(x) + f(x - \Delta x)}{\Delta x^2} \tag{A.2}$$

A.2 Eigen mode equation

When we try to propagate the light through the waveguide, we need to know the Mode profile, effective index and related information to explain the critical characteristics of the opto-electronic device. Here, we try to solve the wave equations numerically to obtain the absorption coefficient, refractive index, 1/e hight and 1/e width and complete mode profile distribution.

The medium with the relative permittivity ϵ_r, the vectorial wave equation for electric field **E** is,

$$\nabla^2\mathbf{E} + \nabla(\frac{\nabla\epsilon_r}{\epsilon_r}.\mathbf{E}) + k_0^2\epsilon_r\mathbf{E} = 0 \tag{A.3}$$

The above equation can be reduced to helmholtz equation if ϵ_r is considered to be constant.

The middle term can be written as,

$$\nabla(\frac{\nabla\epsilon_r}{\epsilon_r}.\mathbf{E}) = \nabla(\frac{1}{\epsilon_r}\frac{\partial\epsilon_r}{\partial x}E_x + \frac{1}{\epsilon_r}\frac{\partial\epsilon_r}{\partial y}E_y) \tag{A.4}$$

Expanding the above equation in X and Y directions,

$$\frac{\partial^2 E_x}{\partial x^2} + \frac{\partial^2 E_x}{\partial y^2} + \frac{\partial^2 E_x}{\partial z^2} + \frac{\partial}{\partial x}(\frac{1}{\epsilon_r}\frac{\partial\epsilon_r}{\partial x}E_x) + \frac{\partial}{\partial x}(\frac{1}{\epsilon_r}\frac{\partial\epsilon_r}{\partial y}E_y) + +k_0^2\epsilon_r E_x = 0 \tag{A.5}$$

and

$$\frac{\partial^2 E_y}{\partial x^2} + \frac{\partial^2 E_y}{\partial y^2} + \frac{\partial^2 E_y}{\partial z^2} + \frac{\partial}{\partial y}(\frac{1}{\epsilon_r}\frac{\partial\epsilon_r}{\partial x}E_x) + \frac{\partial}{\partial y}(\frac{1}{\epsilon_r}\frac{\partial\epsilon_r}{\partial y}E_y) + k_0^2\epsilon_r E_y = 0 \tag{A.6}$$

The above equations can be simplified by combining 1st and 4th term in (2.17) and 2nd and 5th terms in equation (2.18) ,

$$\frac{\partial}{\partial x}(\frac{1}{\epsilon_r}\frac{\partial}{\partial x}(\epsilon_r E_x)) + \frac{\partial^2 E_x}{\partial y^2} + \frac{\partial^2 E_x}{\partial z^2} + k_0^2\epsilon_r E_x + \frac{\partial}{\partial x}(\frac{1}{\epsilon_r}\frac{\partial\epsilon_r}{\partial y}E_y) = 0 \tag{A.7}$$

and

$$\frac{\partial^2 E_y}{\partial x^2} + \frac{\partial}{\partial y}(\frac{1}{\epsilon_r}\frac{\partial}{\partial y}(\epsilon_r E_y)) + \frac{\partial^2 E_y}{\partial z^2} + k_0^2\epsilon_r E_y + \frac{\partial}{\partial y}(\frac{1}{\epsilon_r}\frac{\partial\epsilon_r}{\partial x}E_x) = 0 \tag{A.8}$$

For magnetic field,

$$\nabla^2\mathbf{H} + \frac{\nabla\epsilon_r}{\epsilon_r} \times (\nabla \times \mathbf{H}) + k_0^2\epsilon_r\mathbf{H} = 0 \tag{A.9}$$

The above equation can be reduced to helmholtz equation if ϵ_r is considered to be constant.

The middle term can be expanded as,

$$\frac{\nabla\epsilon_r}{\epsilon_r} \times (\nabla \times \mathbf{H}) = \begin{vmatrix} i & j & k \\ \frac{\partial\epsilon_r}{\partial x} & \frac{\partial\epsilon_r}{\partial y} & 0 \\ (\nabla \times H)_x & (\nabla \times H)_y & (\nabla \times H)_z \end{vmatrix} \tag{A.10}$$

ϵ_r is independent of z direction and hence it is taken as 0. The above equation can be rewrite as,

$$\begin{aligned} \frac{\nabla\epsilon_r}{\epsilon_r} \times (\nabla \times \mathbf{H}) = \frac{\partial\epsilon_r}{\partial y}(\nabla \times H)_z i - \frac{\partial\epsilon_r}{\partial x}(\nabla \times H)_z j + \\ (\frac{\partial\epsilon_r}{\partial x}(\nabla \times H)_y - \frac{\partial\epsilon_r}{\partial y}(\nabla \times H)_x)k \end{aligned} \tag{A.11}$$

Using the below expressions,

$$(\nabla \times \mathbf{H})_x = \frac{\partial H_z}{\partial y} - \frac{\partial H_y}{\partial z} \tag{A.12}$$

$$(\nabla \times \mathbf{H})_y = \frac{\partial H_x}{\partial z} - \frac{\partial H_z}{\partial x} \tag{A.13}$$

$$(\nabla \times \mathbf{H})_z = \frac{\partial H_y}{\partial x} - \frac{\partial H_x}{\partial y} \tag{A.14}$$

We can expand the wave equations as,

$$\begin{aligned} \frac{\nabla\epsilon_r}{\epsilon_r} \times (\nabla \times \mathbf{H}) = \frac{1}{\epsilon_r}(\frac{\partial\epsilon_r}{\partial y}(\frac{\partial H_y}{\partial x} - \frac{\partial H_x}{\partial y})i - \frac{\partial\epsilon_r}{\partial x}(\frac{\partial H_y}{\partial x} - \frac{\partial H_x}{\partial y})j \\ + \left(\frac{\partial\epsilon_r}{\partial x}(\frac{\partial H_x}{\partial z} - \frac{\partial H_z}{\partial x}) - \frac{\partial\epsilon_r}{\partial y}(\frac{\partial H_z}{\partial y} - \frac{\partial H_y}{\partial z})\right)k) \end{aligned} \tag{A.15}$$

Substituting equation (2.27) into (2.21) and splitting into X and Y components, we can split the wave equation as ,

$$\frac{\partial^2 H_x}{\partial x^2} + \frac{\partial^2 H_x}{\partial y^2} + \frac{\partial^2 H_x}{\partial z^2} + \frac{1}{\epsilon_r}\frac{\partial\epsilon_r}{\partial y}(\frac{\partial H_y}{\partial x} - \frac{\partial H_x}{\partial y}) + k_0^2\epsilon_r H_x = 0 \tag{A.16}$$

which can be written by combining 2nd and 5th terms as,

$$\frac{\partial^2 H_x}{\partial x^2} + \epsilon_r \frac{\partial}{\partial y}(\frac{1}{\epsilon_r}\frac{\partial H_y}{\partial y}) + \frac{\partial^2 H_x}{\partial z^2} + k_0^2 \epsilon_r H_x + \frac{1}{\epsilon_r}\frac{\partial \epsilon_r}{\partial y}(\frac{\partial H_y}{\partial x}) = 0 \tag{A.17}$$

and the Y component can be written as

$$\frac{\partial^2 H_y}{\partial x^2} + \frac{\partial^2 H_y}{\partial y^2} + \frac{\partial^2 H_y}{\partial z^2} - \frac{1}{\epsilon_r}\frac{\partial \epsilon_r}{\partial x}(\frac{\partial H_y}{\partial x} - \frac{\partial H_x}{\partial y}) + k_0^2 \epsilon_r H_y = 0 \tag{A.18}$$

which can be rewritten by combining 1st and 3rd terms as,

$$\epsilon_r \frac{\partial}{\partial x}(\frac{1}{\epsilon_r}\frac{\partial H_y}{\partial x}) + \frac{\partial^2 H_y}{\partial y^2} + \frac{\partial^2 H_y}{\partial z^2} + k_0^2 \epsilon_r H_y + \frac{1}{\epsilon_r}\frac{\partial \epsilon_r}{\partial x}(\frac{\partial H_x}{\partial y}) = 0 \tag{A.19}$$

For a wave propagating in z direction,

$$\frac{\partial}{\partial z} = -j\beta \tag{A.20}$$

Substituting (2.32) into (2.19),(2.20),(2.29),(2.31) and rewriting the wave equations,

$$\boxed{\begin{aligned}
\frac{\partial}{\partial x}\big(\frac{1}{\epsilon_r}\frac{\partial}{\partial x}(\epsilon_r E_x)\big) + \frac{\partial^2 E_x}{\partial y^2} + (k_0^2\epsilon_r - \beta^2)E_x + \frac{\partial}{\partial x}\big(\frac{1}{\epsilon_r}\frac{\partial \epsilon_r}{\partial y}E_y\big) &= 0 \\
\frac{\partial^2 E_y}{\partial x^2} + \frac{\partial}{\partial y}(\frac{1}{\epsilon_r}\frac{\partial}{\partial y}(\epsilon_r E_y)) + (k_0^2\epsilon_r - \beta^2)E_y + \frac{\partial}{\partial y}(\frac{1}{\epsilon_r}\frac{\partial \epsilon_r}{\partial x}E_x) &= 0 \\
\frac{\partial^2 H_x}{\partial x^2} + \epsilon_r \frac{\partial}{\partial y}(\frac{1}{\epsilon_r}\frac{\partial H_y}{\partial y}) + (k_0^2\epsilon_r - \beta^2)H_x + \frac{1}{\epsilon_r}\frac{\partial \epsilon_r}{\partial y}(\frac{\partial H_y}{\partial x}) &= 0 \\
\epsilon_r \frac{\partial}{\partial x}(\frac{1}{\epsilon_r}\frac{\partial H_y}{\partial x}) + \frac{\partial^2 H_y}{\partial y^2} + (k_0^2\epsilon_r - \beta^2)H_y + \frac{1}{\epsilon_r}\frac{\partial \epsilon_r}{\partial x}(\frac{\partial H_x}{\partial y}) &= 0
\end{aligned}} \tag{A.21}$$

As we see, the set of equations mentioned in (2.33) are coupled. The first two equations indicate the electric field variation in both directions. Similarly, 3rd and 4th

equations show the magnetic field variation.

Usually, the terms $\frac{\partial}{\partial x}(\frac{1}{\epsilon_r}\frac{\partial \epsilon_r}{\partial y}E_y)$,$\frac{\partial}{\partial y}(\frac{1}{\epsilon_r}\frac{\partial \epsilon_r}{\partial x}E_x)$,$\frac{1}{\epsilon_r}\frac{\partial \epsilon_r}{\partial y}(\frac{\partial H_y}{\partial x})$,$\frac{1}{\epsilon_r}\frac{\partial \epsilon_r}{\partial x}(\frac{\partial H_x}{\partial y})$ are small. By neglecting these terms, we get semivectorial wave equations which are now decoupled and can be solved.

$$\boxed{\begin{aligned}
\frac{\partial}{\partial x}\big(\frac{1}{\epsilon_r}\frac{\partial}{\partial x}(\epsilon_r E_x)\big) + \frac{\partial^2 E_x}{\partial y^2} + (k_0^2\epsilon_r - \beta^2)E_x = 0 \\
\frac{\partial^2 E_y}{\partial x^2} + \frac{\partial}{\partial y}(\frac{1}{\epsilon_r}\frac{\partial}{\partial y}(\epsilon_r E_y)) + (k_0^2\epsilon_r - \beta^2)E_y = 0 \\
\frac{\partial^2 H_x}{\partial x^2} + \epsilon_r\frac{\partial}{\partial y}(\frac{1}{\epsilon_r}\frac{\partial H_y}{\partial y}) + (k_0^2\epsilon_r - \beta^2)H_x = 0 \\
\epsilon_r\frac{\partial}{\partial x}(\frac{1}{\epsilon_r}\frac{\partial H_y}{\partial x}) + \frac{\partial^2 H_y}{\partial y^2} + (k_0^2\epsilon_r - \beta^2)H_y = 0
\end{aligned}} \tag{A.22}$$

This approximation can be used if the interaction of the field components in one direction is negligible in other direction. These can be analyzed considering quasi TE or quasi TM modes which have E_x and H_y or E_y and H_x as their field components.

Therefore TE wave equation as per above discussion can be written as,

$$\frac{\partial}{\partial x}\big(\frac{1}{\epsilon_r}\frac{\partial}{\partial x}(\epsilon_r E_x)\big) + \frac{\partial^2 E_x}{\partial y^2} + (k_0^2\epsilon_r - \beta^2)E_x = 0 \tag{A.23}$$

and TM wave equation is,

$$\frac{\partial^2 E_y}{\partial x^2} + \frac{\partial}{\partial y}(\frac{1}{\epsilon_r}\frac{\partial}{\partial y}(\epsilon_r E_y)) + (k_0^2\epsilon_r - \beta^2)E_y = 0 \tag{A.24}$$

Considering TE wave equations,using the finite difference scheme assuming uniform mesh size throughout the structure. If we consider that (i,j) as the node that represents the point of the region at a distance of $i \times h$ horizontal direction and $j \times h$ from vertical direction , these can be rewritten as,

$$\begin{aligned}
\frac{\partial^2 E_x}{\partial x^2} &= \frac{E(i+1,j) + E(i-1,j) - 2E(i,j)}{h^2} \\
\frac{\partial^2 E_x}{\partial y^2} &= \frac{E(i,j+1) + E(i,j-1) - 2E(i,j)}{h^2}
\end{aligned} \tag{A.25}$$

Table A.1: Coefficients of semivectorial wave equations

	TE Polarization	**TM Polarization**
A	$\frac{2\epsilon_r(i+1,j)}{\epsilon(i+1,j)+\epsilon(i,j)}\frac{1}{(k_0\times h)^2}$	$\frac{1}{(k_0\times h)^2}$
B	$\frac{2\epsilon_r(i-1,j)}{\epsilon(i-1,j)+\epsilon(i,j)}\frac{1}{(k_0\times h)^2}$	$\frac{1}{(k_0\times h)^2}$
C	$\frac{1}{(k_0\times h)^2}$	$\frac{2\epsilon_r(i,j+1)}{\epsilon(i,j+1)+\epsilon(i,j)}\frac{1}{(k_0\times h)^2}$
D	$\frac{1}{(k_0\times h)^2}$	$\frac{2\epsilon_r(i,j-1)}{\epsilon(i,j-1)+\epsilon(i,j)}\frac{1}{(k_0\times h)^2}$
F	$\epsilon_r(i,j) - 2(1 + \epsilon_r(i,j))(\frac{1}{\epsilon_r(i+1,j)+\epsilon_r(i,j)} + \frac{1}{\epsilon_r(i-1,j)+\epsilon_r(i,j)})$	$\epsilon_r(i,j) - 2(1 + \epsilon_r(i,j))(\frac{1}{\epsilon_r(i+1,j)+\epsilon_r(i,j)} + \frac{1}{\epsilon_r(i-1,j)+\epsilon_r(i,j)})$
G	$\beta^2/k_0^2 = n_{eff}^2$	$\beta^2/k_0^2 = n_{eff}^2$

and the other terms can be expanded as,

$$\begin{aligned}\frac{\partial}{\partial x}(\frac{1}{\epsilon_r}\frac{\partial \epsilon_r}{\partial x}E_x) &= \frac{1}{h}\left(\left(\frac{1}{\epsilon_r}\frac{\partial \epsilon_r}{\partial x}E_x\right)_{p+1/2,q} - \left(\frac{1}{\epsilon_r}\frac{\partial \epsilon_r}{\partial x}E_x\right)_{p-1/2,q}\right) \\ &= \frac{1}{h^2}\left(\frac{\epsilon_r(i+1,j)-\epsilon_r(i,j)}{\epsilon_r(i+1,j)+\epsilon_r(i,j)}(E(i+1,j)+E(i,j)) - \right. \\ &\qquad \left. \frac{\epsilon_r(i,j)-\epsilon_r(i-1,j)}{\epsilon_r(i,j)+\epsilon_r(i-1,j)}(E(i-1,j)+E(i,j))\right)\end{aligned} \tag{A.26}$$

Substituting the equations (2.37) and (2.38) into (2.36) and rearranging the terms we get,

$$AE(i+1,j)+BE(i-1,j)+CE(i,j+1)+DE(i,j-1)+FE(i,j) = GE(i,j) \tag{A.27}$$

where A,B,C,D,F,G are the coefficients explained above for both TE and TM polarizations.

A.3 Coefficients of Poisson equation

The potential for solving poisson equation is taken as $V+\delta$ and substituted into Poisson equation 2.8 [13], we get

$$\begin{aligned}
&\delta(i+1,j)+\delta(i-1,j)+\delta(i,j-1)+\delta(i,j+1)-4\delta(i,j)\\
&+V(i+1,j)+V(i-1,j)+V(i,j-1)+V(i,j+1)-4V(i,j)\\
&=\frac{-q(n_i e^{\frac{(E_i-E_f)}{kT}}-n_i e^{\frac{(E_f-E_i)}{kT}}+N_D(i,j)-N_A(i,j))\times h^2}{\epsilon}
\end{aligned} \tag{A.28}$$

We consider E_f as the reference in above equation. Since

$$E_i = -q \times V \tag{A.29}$$

we can rewrite the equation (2.13) as,

$$\begin{aligned}
&\delta(i+1,j)+\delta(i-1,j)+\delta(i,j-1)+\delta(i,j+1)-4\delta(i,j)\\
&+V(i+1,j)+V(i-1,j)+V(i,j-1)+V(i,j+1)-4V(i,j)\\
&=\frac{-q(n_i e^{\frac{(-V-\delta)}{V_t}}-n_i e^{\frac{(V+\delta)}{V_t}}+N_D(i,j)-N_A(i,j))\times h^2}{\epsilon}
\end{aligned} \tag{A.30}$$

Normalizing with respect to V_t, by the transformations $\frac{V}{V_t}=V$; $\frac{\delta}{V_t}=\delta$ we get,

$$\begin{aligned}
&\delta(i+1,j)+\delta(i-1,j)+\delta(i,j-1)+\delta(i,j+1)-4\delta(i,j)\\
&+V(i+1,j)+V(i-1,j)+V(i,j-1)+V(i,j+1)-4V(i,j)\\
&=\frac{-q(n_i e^{(-V-\delta)}-n_i e^{(V+\delta)}+N_D(i,j)-N_A(i,j))\times h^2}{\epsilon V_t}
\end{aligned} \tag{A.31}$$

We assume that δ is too small compared with the voltage V and hence we can rewrite above equation as,

$$\begin{aligned}
&\delta(i+1,j)+\delta(i-1,j)+\delta(i,j-1)+\delta(i,j+1)-4\delta(i,j)\\
&+V(i+1,j)+V(i-1,j)+V(i,j-1)+V(i,j+1)-4V(i,j)\\
&=\frac{-qh^2}{\epsilon V_t}(n_i e^{-V(i,j)}(1-\delta(i,j))-n_i e^{V(i,j)}(1+\delta(i,j))+N_D(i,j)-N_A(i,j))
\end{aligned} \tag{A.32}$$

Rearranging the terms,

$$\begin{aligned}\delta(i+1,j)+\delta(i-1,j)+\delta(i,j-1)+\delta(i,j+1)+\delta(i,j)(-4-\frac{qh^2n_i}{\epsilon V_t}(e^{-V(i,j)}+e^{V(i,j)}))\\ +V(i+1,j)+V(i-1,j)+V(i,j-1)+V(i,j+1)-4V(i,j)\\ =\frac{-qh^2}{\epsilon V_t}(n_ie^{-V(i,j)}-n_ie^{V(i,j)}+N_D(i,j)-N_A(i,j))\end{aligned} \tag{A.33}$$

is of the form,

$$\begin{aligned}a(i,j)\delta(i-1,j)+b(i,j)\delta(i,j)+c(i,j)\delta(i+1,j)\\ +d(i,j)\delta(i,j-1)+e(i,j)\delta(i,j+1)=k(i,j)\end{aligned} \tag{A.34}$$

The matrices a, b, c, d, e are 2 dimensional and are either constants or function of potential from previous iteration.

The following table consists of the coefficients a, b, c, d, e, k for all types of regions we process.

Table A.2: Coefficients of Poisson equation for all processing regions

Coefficient	Conductor	Semiconductor	Insulator
a	0	1	1
b	1	$(-4-\frac{qh^2n_i}{\epsilon V_t}(e^{-V(i,j)}+e^{V(i,j)}))$	-4
c	0	1	1
d	0	1	1
e	0	1	1
k	0	$\frac{-qh^2}{\epsilon V_t}(n_ie^{-V(i,j)}-n_ie^{V(i,j)}+N_D(i,j)-N_A(i,j))$+ 4V(i,j)-V(i-1,j)-V(i+1,j)-V(i,j-1)-V(i,j+1)	4V(i,j)-V(i-1,j)-V(i+1,j)-V(i,j-1)-V(i,j+1)

REFERENCES

[1] G.T. Reed and Andrew. P. Knights, "Silicon Photonics - An Introduction", 1st edition, pages-73,101-102, Wiley publications, 2004.

[2] P. Sakthivel, N. Dasgupta, and B.K. Das, "Simulation and experimental studies of diffusion doped p-i-n structures for silicon photonics." *SPIE Photonics West 2013 pages 8629-8633*, 2013.

[3] Cutolo, Antonello, et al. "Silicon electro-optic modulator based on a three terminal device integrated in a low-loss single-mode SOI waveguide." *Journal of Lightwave Technology, vol. 15, no. 3* (1997): 505-518.

[4] Liu, Ansheng, et al. "A high-speed silicon optical modulator based on a metal-oxide-semiconductor capacitor." *Nature, vol. 427, no. 6975* (2004): 615-618.

[5] Feng, Ning-Ning, et al. "High speed carrier-depletion modulators with 1.4 V-cm V_{π}L integrated on 0.25 μm silicon-on-insulator waveguides." *Opt. Express, vol. 18, no. 8* (2010): 7994-7999.

[6] Soref, Richard A., Joachim Schmidtchen, and Klaus Petermann. "Large single-mode rib waveguides in GeSi-Si and Si-on-SiO_2.", *IEEE Journal of Quantum Electronics, vol. 27, no. 8* (1991): 1971-1974.

[7] Matthew. N. O. Sadiku, “Elements of electromagnetics”, 3rd edition, chapter 4 and 5, pages 103-182.

[8] Matthew. N. O. Sadiku, “Numerical Techniques in electromagnetics with MATLAB”, 3rd edition, Chapter 3, pages 119-135, 2011.

[9] Jozwikowska, Alina. "Numerical solution of the nonlinear Poisson equation for semiconductor devices by application of a diffusion-equation finite difference scheme." *Journal of Applied Physics, vol. 104, no. 6* (2008): 063715-063715

[10] Kenji Kawano and Tsutomu Kitoh, “Introduction to Optical Waveguide Analysis -Solving Maxwell’s equations and Schrodinger equation”, chapter 4, pages 119-159, Wiley publicaions 2001.

[11] Ben Streetman and Sanjay Banerjee, “Solid state electronic devices”, sixth edition, chapter 4, pages 124-147, PHL learning private limited, 2009.

[12] Scharfetter, D. L., and H. K. Gummel. "Large signal analysis of a Silicon Read diode oscillator.", *IEEE Transactions on Electron devices, vol. 16, no. 1* (1969):64-77.

[13] Dragica Vasileska, Stephen M.Goodnick, Gerhard Klimeck,”Computational Electronics Semiclassical and Quantum Device Modelling and Simulation” , CRC Press , 2010 , pages: 154-156,171-176

[14] C.M.Snowden, “Semiconductor device modelling,”chapter 5, pages 95-115, 1988.

[15] Cebin P. Sebastian. "Numerical Analysis in Integrated Optoelectronics: Modesolver and Analysis." IOLAB, IIT Madras,chapter 5 , May 2012.

[16] TCAD Medici User Guide